Asymptotically flat hairy black holes in massive bigravity

Romain Gervalle[1,*] and Mikhail S. Volkov[1,2,3,†]

[1]*Institut Denis Poisson, UMR - CNRS 7013, Université de Tours, Parc de Grandmont, 37200 Tours, France*

[2]*Institute for Theoretical and Mathematical Physics, Lomonosov Moscow State University, Leninskie Gory, GSP-1, 119991 Moscow, Russia*

[3]*Department of General Relativity and Gravitation, Institute of Physics, Kazan Federal University, Kremlevskaya street 18, 420008 Kazan, Russia*

(Received 10 September 2020; accepted 19 November 2020; published 17 December 2020)

We study asymptotically flat black holes with massive graviton hair within the ghost-free bigravity theory. There have been contradictory statements in the literature about their existence—such solutions were reported some time ago, but later a different group claimed the Schwarzschild solution to be the only asymptotically flat black hole in the theory. As a result, the controversy emerged. We have analyzed the issue ourselves and have been able to construct such solutions within a carefully designed numerical scheme. We find that for given parameter values there can be one or two asymptotically flat hairy black hole solutions in addition to the Schwarzschild solution. We analyze their perturbative stability and find that they can be stable or unstable, depending on the parameter values. The masses of stable hairy black holes that would be physically relevant range form stellar values up to values typical for supermassive black holes. One of their two metrics is extremely close to Schwarzschild, while all their "hair" is hidden in the second metric that is not coupled to matter and not directly seen. If the massive bigravity theory indeed describes physics, the hair of such black holes should manifest themselves in violent processes like black hole mergers and should be visible in the structure of the signals detected by LIGO/VIRGO.

DOI: 10.1103/PhysRevD.102.124040

I. INTRODUCTION

Theories with massive gravitons provide a natural modification of the general relativity (GR) in the infrared regime and can be used to explain the current acceleration of our Universe [1,2]. Such theories have a long history pioneered by the work of Fierz and Pauli [3] and marked by subsequent discoveries of many interesting features, such as the vDVZ discontinuity [4,5], the Vainshtein mechanism [6], the Boulware-Deser ghost [7], culminating in the discovery of the ghost-free massive gravity [8] and ghost-free bigravity [9] theories.

The ghost-free bigravity theory is the most interesting physically. It contains two dynamical metrics, usually called $g_{\mu\nu}$ and $f_{\mu\nu}$, describing together two gravitons, one of which is massive and the other is massless. The theory admits self-accelerating cosmological solutions [10–12] whose properties can agree with the observations [13–17], with the Λ term mimicked by the graviton mass. The theory also admits solutions describing black holes [18], wormholes [19], and other interesting solutions (see [20] for a review). In what follows we shall be discussing black holes.

The bigravity black holes can be either "bald" or "hairy." The bald black holes are described by the known GR metrics. Such solutions were first discovered long ago [21–23] within the old bigravity theory inspired by physics of strong interactions [24]. In the simplest case, their two metrics are both Schwarzschild–(anti-)de Sitter and can be conveniently represented in the Eddington-Finkelstein coordinates as [25,26]

$$g_{\mu\nu}dx^\mu dx^\nu = -\Sigma_g dv^2 + 2dvdr + r^2 d\Omega^2,$$
$$f_{\mu\nu}dx^\mu dx^\nu = C^2(-\Sigma_f dv^2 + 2dvdr + r^2 d\Omega^2), \tag{1.1}$$

with $\Sigma_g = 1–2M_g/r + \Lambda_g/(3r^2)$ and $\Sigma_f = 1–2M_f/r + \Lambda_f/(3r^2)$, where values of constants C, Λ_g, Λ_f are fixed by the field equations. Passing to the Schwarzschild coordinates, one can diagonalize one of the two metrics, but not both of them simultaneously. Such solutions have been much studied [27]; they exist also within the ghost-free bigravity [28], and they admit the charged [29] and

*romain.gervalle@univ-tours.fr
†volkov@lmpt.univ-tours.fr

spinning [30] generalizations. These solutions also admit the massive gravity limit where $M_f = \Lambda_f = 0$ hence the f metric is flat while the g metric remains nontrivial, and this yields all possible static black holes in the ghost-free massive gravity theory (it seems there can be also time-dependent black holes in this theory [31]).

Next, it was noticed in [18] that if the parameters of the potential are suitably adjusted, then the ghost-free bigravity reduces to the vacuum GR when the two metrics coincide, $g_{\mu\nu} = f_{\mu\nu}$. Therefore, all vacuum black holes, as for example the Schwarzschild solution (to be called bald to distinguish it from the "hairy Schwarzschild" to be described below),

$$g_{\mu\nu}dx^\mu dx^\nu = f_{\mu\nu}dx^\mu dx^\nu = -\left(1-\frac{2M}{r}\right)dt^2 + \frac{dr^2}{1-2M/r} + r^2 d\Omega^2, \tag{1.2}$$

or its spinning generalization can be imbedded into the ghost-free bigravity. A Λ term can be included by assuming the two metrics to be proportional to each other [18,20,26]. Such solutions are different from solutions of type (1.1), for example they do not admit the massive gravity limit. In addition, the solution (1.1) is linearly stable [32], whereas (1.2) is unstable (for a small M) with respect to fluctuations which do not respect the condition $g_{\mu\nu} = f_{\mu\nu}$ [33].

These facts essentially exhaust the available knowledge of the bald black holes in the bigravity theory. At the same time, more general hairy black holes not described by the classical GR metrics can exist as well. The first example of hairy black holes in physics was found long ago [34], followed by many other examples (see [35,36] for a review), so that nowadays hairy black holes are considered as something usual. One may therefore wonder if they exist in the ghost-free bigravity theory as well.

A systematic analysis of hairy black holes in the ghost-free massive bigravity has been carried out for the first time by one of the authors [18], but none of the solutions found were asymptotically flat. In that analysis both metrics were assumed to be static and spherically symmetric. If they are not simultaneously diagonal, then the most general solution is given by (1.1). If they are simultaneously diagonal, then one of the solutions is given by (1.2), but other more general black hole solutions exist as well.

Such solutions possess an event horizon—a hypersurface that is null simultaneously with respect to $g_{\mu\nu}$ and $f_{\mu\nu}$. Therefore, both metrics share the horizon [37,38], but its radius r_H^g measured by $g_{\mu\nu}$ can be different from the radius r_H^f measured by $f_{\mu\nu}$. One can set $r_H \equiv r_H^g$ to unit value via rescaling the system (rescaling at the same time the graviton mass), but the ratio $u = r_H^g/r_H^f$ is scale invariant. Choosing a value of u completely determines the boundary conditions at the horizon, which allows one to integrate the equations starting from the horizon toward large values of the radial coordinate r. As a result, the set of all black hole solutions can be labeled by just one parameter u, and integrating the equations for different values of u gives all possible black holes.

Choosing $u = 1$ yields the Schwarzschild solution (1.2). For $u \neq 1$ one finds more general black holes supporting a massive graviton "hair" outside the horizon, but in the asymptotic region their two geometries do not become flat [18]. The latter property is generic, and trying different values of u always gives either solutions with a curvature singularity somewhere outside the horizon, or solutions which exist for all values of r but show nonflat asymptotics.

At the same time, these facts do not completely exclude a possibility of some other asymptotically flat black hole solutions different from (1.2), which would correspond to some special values of u different from $u = 1$. However, even if they exist, one does not find such solutions by a brute force via trying many different values of u, and the reason is the following. The field equations reduce to three coupled first order ordinary differential equations (ODEs) [18], whose *local* at large r solution has schematically the following structure when it is linearized around flat space (A, B, C being integration constants):

$$\frac{A}{r} + Be^{-r} + Ce^{+r}. \tag{1.3}$$

Here $r = \mathrm{m}\mathrm{r}$ is the dimensionless radial coordinate, with m and r being the graviton mass and dimensionful radial coordinate (we assume the graviton mass to have the dimension of inverse length, so that this is rather the inverse Compton wavelength $\mathrm{m}c/\hbar$). The Newtonian mode A/r in (1.3) arises due to the massless graviton present in the theory, while the decaying mode Be^{-r} and the growing mode Ce^{+r} are due to the massive graviton. Now, when integrating from the horizon, the growing mode Ce^{+r} will be inevitably present in the numerical solution at large r and will drive the solution away from flat space. This is why one does not find asymptotically flat solutions in this way.

To get them, one should suppress the growing mode by setting $C = 0$, hence the local solutions at large r will comprise a two-parameter set labeled by A and B. The next step is to numerically extend this local solution toward small r, extending at the same time the local solution at the horizon labeled by u toward large r, until the two solutions meet at some intermediate point. For these solutions to agree, three (the number of the ODEs) matching conditions should be satisfied via adjusting the three parameters u, A, B. In practice, this can be done within the numerical multiple-shooting method [39]. Once u, A, B are adjusted, this yields global asymptotically flat solutions.

The difficulty, however, is that the numerical scheme requires some input values for u, A, B, which should be close to the "true values," otherwise the iterations do not

converge. It was *a priori* unclear how to choose these input values, whereas choosing them randomly does not give the convergence. Some additional information was needed to properly choose these input values, but at the time of writing the article [18] such information was not available. As a result, the conclusion of that work was that asymptotically flat hairy black holes may exist, but they should be parametrically isolated form the Schwarzschild solution (1.2).

It is interesting that by adding an extra matter source to obtain not a black hole but a regular object like a star, asymptotically flat solutions can be easily constructed, as was shown first in [18] and later in [40,41]. The black hole case is more difficult.

Fortunately, the additional information was later obtained within the analysis of perturbations of the Schwarzschild solution (1.2) [33,42]. Denoting $g^S_{\mu\nu}$ the Schwarzschild metric, the two perturbed metrics are $g_{\mu\nu} = g^S_{\mu\nu} + \delta g_{\mu\nu}$ and $f_{\mu\nu} = g^S_{\mu\nu} + \delta f_{\mu\nu}$. Linearizing the field equations with respect to $\delta g_{\mu\nu}$ and $\delta f_{\mu\nu}$, one finds that perturbations grow in time and hence the background Schwarzschild black hole is unstable if $r_H \equiv \mathrm{mr_H} \leq 0.86$. On the other hand, for $r_H > 0.86$ the perturbations are bounded in time so that the background is stable [33]. Curiously, the mathematical structure of the perturbation equations is identical [33] to that previously discovered by Gregory and Laflamm (GL) in their analysis of black strings in $D = 5$ GR [43]. We shall therefore refer to the Schwarzschild solution with $r_H = 0.86$ as GL point.

This change of stability at the GL point suggests that for r_H close to 0.86 there could be two different asymptotically flat solutions: the Schwarzschild solution (1.2) and also some other solution which can be approximated by the zero perturbation mode that exists at the GL point. This new solution is different from Schwarzschild although close to it, hence it describes an asymptotically flat hairy black hole. To get this solution within the numerical scheme outlined above, one should choose the input parameters u, A, B to be close the GL point, $u \approx 1$, $r_H \approx 0.86$, $A \approx -r_H/2$, $B \approx 0$, and it is this essential piece of information that was missing when writing Ref. [18]. As soon as the solution is obtained, one can change the value of r_H iteratively, thus obtaining "fully fledged" hairy black holes which may deviate considerably from the parent Schwarzschild solution.

Remarkably, this program was accomplished by the Portuguese group [44] via explicitly constructing asymptotically flat hairy black holes in the theory in the region *below* the GL point, for $r_H < 0.86$. However, some time later spherically symmetric bigravity solutions were analyzed by the Swedish group [45], and it was claimed that the Schwarzschild solution (1.2) represents the unique asymptotically flat black hole in the theory. As a result, a controversy emerged and it was unclear if asymptotically flat hairy black holes exist or not.

We have therefore reconsidered the issue ourselves and below are our results. In brief, we were able to construct asymptotically flat hairy black holes in the theory, thereby confirming the finding of [44]. We apply a very carefully designed numerical scheme to exclude any ambiguities and to take into account the arguments of [45]. In fact, these arguments correctly point to some drawbacks of the numerical analysis commonly present in many publications. From the mathematical viewpoint, one has to solve a nonlinear boundary value problem where the boundaries are singular points of the differential equations (horizon and infinity). Since it is difficult to approach such points numerically, various approximations are used in practice, which may give reasonable results in some cases but inevitably increase the numerical errors and lead to a numerical instability. Only very rarely does one find in the literature a correct treatment of the problem (apart from the relaxation approach), as for example in [46–48]. We therefore pay special attention to the details of our numerical scheme and describe them in a very explicit way. From the methodological viewpoint, our paper gives an example of how one should properly tackle a nonlinear boundary value problem with singular endpoints.

We cross-check our results with two different numerical codes written independently by two of us. Our results strongly suggest that the hairy solutions exist and are indeed asymptotically flat and regular. We discover many new features of these solutions, for example we obtain hairy black holes also *above* the GL point for $r_H > 0.86$, and we study for the first time the perturbative stability of the solutions. We were able to identify regions in the parameter space which correspond to stable solutions, and we determined subsets of these regions which agree with the constraints imposed by the cosmological observations. We find that the viable hairy black holes should be described by the g metric that is very close to Schwarzschild, but their f metric is different. Therefore, if the bigravity theory indeed describes physics, the astrophysical black holes should hide the hair in their f metric. We find masses of such black holes to range from $\sim 0.2\ \mathrm{M}_\odot$ to $\sim 0.3 \times 10^6\ \mathrm{M}_\odot$.

We have also attentively considered the arguments of Ref. [45]. In brief, this work seems to agree that the hairy solutions exist but judges them physically unacceptable. We analyze the arguments and we think some of them are interesting and should be taken into consideration, but none of them is decisive, so that they should rather be viewed as a conjecture. To understand its origin, we notice that the numerical procedure adopted in that work is not suitable for suppressing the growing at infinity mode, which generates artificial numerical singularities. This must be the reason why the solutions were judged unacceptable in that work. However, no singularities appear within the properly chosen numerical scheme, and we specially adapt our scheme to be able to cope with the arguments of [45].

We shall postpone a more detailed discussion of Ref. [45] until the end of this text to be able to make a comparison with our results.

The rest of the text is organized as follows. In Sec. II we introduce the massive bigravity theory of Hassan and Rosen [9]. The field equations, their reduction to the static and spherically symmetric sector, and the simplest solutions are described in Secs. III–V. In Secs. VI and VII we describe in detail our analysis of boundary conditions at the horizon and at infinity, and then summarize in Sec. VIII the structure of our numerical procedure. In Sec. IX we show our solutions for asymptotically flat hairy black holes and also describe the duality relation yielding the solutions above the GL point. After that, we discuss in Sec. X the perturbations of the hairy backgrounds and the analysis of the negative perturbation modes. Our discussion culminates in Sec. XI where we describe various limits and identify regions in the parameter space where the solutions exist and where they are stable. In Sec. XII we give a brief summary of our results and discuss the arguments of Ref. [45]. The two Appendixes contain the description of the desingularization of the equations at the horizon, as well as the complete set of the field equations in the time-dependent case.

II. THE GHOST-FREE BIGRAVITY

The theory is defined on a four-dimensional spacetime manifold endowed with two Lorentzian metrics $\mathrm{g}_{\mu\nu}$ and $\mathrm{f}_{\mu\nu}$ with the signature $(-,+,+,+)$. The action is [9]

$$S[\mathrm{g},\mathrm{f}]=\frac{1}{2\boldsymbol{\kappa}_1}\int R(\mathrm{g})\sqrt{-\mathrm{g}}d^4\mathrm{x}+\frac{1}{2\boldsymbol{\kappa}_2}\int R(\mathrm{f})\sqrt{-\mathrm{f}}d^4\mathrm{x}-\frac{\mathrm{m}^2}{\boldsymbol{\kappa}}\int \mathcal{U}\sqrt{-\mathrm{g}}d^4\mathrm{x}, \tag{2.1}$$

where $\boldsymbol{\kappa}_1$ and $\boldsymbol{\kappa}_2$ are the gravitational couplings, $\boldsymbol{\kappa}$ is a parameter with the same dimension, and m is a mass parameter. The interaction between the two metrics is expressed by a scalar function of the tensor (the hat denotes matrices)

$$\hat{\gamma}=\sqrt{\hat{\mathrm{g}}^{-1}\hat{\mathrm{f}}}. \tag{2.2}$$

Here the matrix square root is understood in the sense that $\hat{\gamma}^2=\hat{\mathrm{g}}^{-1}\hat{\mathrm{f}}$, which can be written in components as

$$(\gamma^2)^\mu{}_\nu\equiv\gamma^\mu{}_\alpha\gamma^\alpha{}_\nu=\mathrm{g}^{\mu\alpha}\mathrm{f}_{\alpha\nu}. \tag{2.3}$$

If λ_a $(a=1,2,3,4)$ are the eigenvalues of $\gamma^\mu{}_\nu$ then the interaction potential is

$$\mathcal{U}=\sum_{n=0}^{4}b_k\mathcal{U}_k, \tag{2.4}$$

where b_k are dimensionless parameters while $\mathcal{U}_k$ are defined by the relations

$$\mathcal{U}_0=1,\qquad \mathcal{U}_1=\sum_a\lambda_a=[\gamma],$$
$$\mathcal{U}_2=\sum_{a<b}\lambda_a\lambda_b=\frac{1}{2!}([\gamma]^2-[\gamma^2]),$$
$$\mathcal{U}_3=\sum_{a<b<c}\lambda_c\lambda_b\lambda_c=\frac{1}{3!}([\gamma]^3-3[\gamma][\gamma^2]+2[\gamma^3]),$$
$$\mathcal{U}_4=\lambda_1\lambda_2\lambda_3\lambda_4=\det(\hat{\gamma}).$$

Here $[\gamma]=\mathrm{tr}(\hat{\gamma})\equiv\gamma^\mu{}_\mu$ and $[\gamma^k]=\mathrm{tr}(\hat{\gamma}^k)\equiv(\gamma^k)^\mu{}_\mu$. The two metrics actually enter the action in a completely symmetric way, since the action is invariant under

$$\mathrm{g}_{\mu\nu}\leftrightarrow\mathrm{f}_{\mu\nu},\qquad \boldsymbol{\kappa}_1\leftrightarrow\boldsymbol{\kappa}_2,\qquad b_k\leftrightarrow b_{4-k}. \tag{2.5}$$

The action is also invariant under rescalings $\boldsymbol{\kappa}\to\pm\lambda^2\boldsymbol{\kappa}$, $b_k\to\pm b_k$, $\mathrm{m}\to\lambda\mathrm{m}$, and this allows one to impose, without any loss of generality, the normalization condition $\boldsymbol{\kappa}=\boldsymbol{\kappa}_1+\boldsymbol{\kappa}_2$. Varying the action with respect to the two metrics gives two sets of Einstein equations,

$$G_{\mu\nu}(\mathrm{g})=\mathrm{m}^2\kappa_1T_{\mu\nu},\qquad G_{\mu\nu}(\mathrm{f})=\mathrm{m}^2\kappa_2\mathcal{T}_{\mu\nu}, \tag{2.6}$$

where $\kappa_1\equiv\boldsymbol{\kappa}_1/\boldsymbol{\kappa}$ and $\kappa_2\equiv\boldsymbol{\kappa}_2/\boldsymbol{\kappa}$, and the normalization of $\boldsymbol{\kappa}$ implies that $\kappa_1+\kappa_2=1$. The source terms in (2.6) are obtained by varying the interaction potential $\mathcal{U}$,

$$T^\mu{}_\nu=\mathrm{g}^{\mu\alpha}T_{\alpha\nu}=\tau^\mu{}_\nu-\mathcal{U}\delta^\mu_\nu,\quad \mathcal{T}^\mu{}_\nu=\mathrm{f}^{\mu\alpha}\mathcal{T}_{\alpha\nu}=-\frac{\sqrt{-\mathrm{g}}}{\sqrt{-\mathrm{f}}}\tau^\mu{}_\nu, \tag{2.7}$$

where $\mathrm{f}^{\mu\alpha}$ is the inverse of $\mathrm{f}_{\mu\alpha}$ and

$$\tau^\mu{}_\nu=\{b_1\mathcal{U}_0+b_2\mathcal{U}_1+b_3\mathcal{U}_2+b_4\mathcal{U}_3\}\gamma^\mu{}_\nu-\{b_2\mathcal{U}_0+b_3\mathcal{U}_1+b_4\mathcal{U}_2\}(\gamma^2)^\mu{}_\nu+\{b_3\mathcal{U}_0+b_4\mathcal{U}_1\}(\gamma^3)^\mu{}_\nu-b_4\mathcal{U}_0(\gamma^4)^\mu{}_\nu. \tag{2.8}$$

There is an identity relation following from the diffeomorphism invariance of the interaction term in the action,

$$\sqrt{-g}\overset{(g)}{\nabla}_\mu T^\mu{}_\nu+\sqrt{-f}\overset{(f)}{\nabla}_\mu\mathcal{T}^\mu{}_\nu\equiv 0, \tag{2.9}$$

where $\overset{(g)}{\nabla}_\rho$ and $\overset{(f)}{\nabla}_\rho$ are the covariant derivatives with respect to $\mathrm{g}_{\mu\nu}$ and $\mathrm{f}_{\mu\nu}$.

Equations (2.6) describe two interacting gravitons, one massive and one massless. This can be easily seen in the flat space limit. Setting $\mathrm{g}_{\mu\nu}=\mathrm{f}_{\mu\nu}=\eta_{\mu\nu}$ (the Minkowski metric), Eqs. (2.6) reduce to

$$0 = -\mathrm{m}^2\kappa_1(P_0 + P_1)\eta_{\mu\nu}, \qquad 0 = -\mathrm{m}^2\kappa_2(P_1 + P_2)\eta_{\mu\nu}, \tag{2.10}$$

with $P_m \equiv b_m + 2b_{m+1} + b_{m+2}$. Therefore, the flat space will be a solution if only the parameters b_k fulfil the conditions $P_1 = -P_0 = -P_2$. Assuming this to be the case, let us set $\mathrm{g}_{\mu\nu} = \eta_{\mu\nu} + \delta\mathrm{g}_{\mu\nu}$ and $\mathrm{f}_{\mu\nu} = \eta_{\mu\nu} + \delta\mathrm{f}_{\mu\nu}$ where the deviations $\delta\mathrm{g}_{\mu\nu}$ and $\delta\mathrm{f}_{\mu\nu}$ are small. Linearizing the equations (2.6) with respect to the deviations yields

$$\hat{\mathcal{E}}^{\alpha\beta}_{\mu\nu} h^{(0)}_{\alpha\beta} = 0, \tag{2.11}$$

$$\hat{\mathcal{E}}^{\alpha\beta}_{\mu\nu} h_{\alpha\beta} + \frac{\mathrm{m}^2_{\mathrm{FP}}}{2}(h_{\mu\nu} - \eta_{\mu\nu}h) = 0, \tag{2.12}$$

where $\hat{\mathcal{E}}^{\alpha\beta}_{\mu\nu}$ denotes the linear part of the Einstein operator, and where $h^{(0)}_{\mu\nu} = \kappa_1\delta\mathrm{f}_{\mu\nu} + \kappa_2\delta\mathrm{g}_{\mu\nu}$ and $h_{\mu\nu} = \delta\mathrm{f}_{\mu\nu} - \delta\mathrm{g}_{\mu\nu}$ with $h = \eta^{\alpha\beta}h_{\alpha\beta}$. The $h^{(0)}_{\mu\nu}$ equations are the linearized Einstein equations describing a massless graviton with two dynamical polarizations. The $h_{\mu\nu}$ field fulfills the Fierz-Pauli equations for massive gravitons with five polarizations and with the mass

$$\mathrm{m}^2_{\mathrm{FP}} = P_1\ \mathrm{m}^2. \tag{2.13}$$

Therefore, one will have $\mathrm{m}_{\mathrm{FP}} = \mathrm{m}$ if

$$P_1 = 1. \tag{2.14}$$

This condition can be solved together with the conditions $P_0 = P_2 = -1$ implied by (2.10) to express the five b_k in terms of two independent parameters, sometimes called c_3 and c_4,

$$b_0 = 4c_3 + c_4 - 6, \qquad b_1 = 3 - 3c_3 - c_4,$$
$$b_2 = 2c_3 + c_4 - 1, \qquad b_3 = -(c_3 + c_4), \qquad b_4 = c_4. \tag{2.15}$$

At the same time, the theory has exactly 7 propagating degrees of freedom also away from the flat space limit and for arbitrary b_k (see [49–51] for its Hamiltonian formulation).

Let us finally pass from the dimensionful spacetime coordinates x^μ to the dimensionless ones,

$$x^\mu = \mathrm{m}\mathrm{x}^\mu. \tag{2.16}$$

This is equivalent to the conformal rescaling of the metrics,

$$\mathrm{g}_{\mu\nu} = \frac{1}{\mathrm{m}^2} g_{\mu\nu}, \qquad \mathrm{f}_{\mu\nu} = \frac{1}{\mathrm{m}^2} f_{\mu\nu}, \tag{2.17}$$

after which the field equations (2.6) reduce to

$$G^\mu{}_\nu(g) = \kappa_1 T^\mu{}_\nu, \qquad G^\mu{}_\nu(f) = \kappa_2 \mathcal{T}^\mu{}_\nu, \tag{2.18}$$

where $T^\mu{}_\nu$ and $\mathcal{T}^\mu{}_\nu$ are still given by (2.7), (2.8) with $\hat{\gamma} = \sqrt{\hat{g}^{-1}\hat{f}}$. The Bianchi identities for these equations imply that

$$\overset{(g)}{\nabla}_\rho T^\rho_\lambda = 0, \qquad \overset{(f)}{\nabla}_\rho \mathcal{T}^\rho_\lambda = 0, \tag{2.19}$$

which is consistent with (2.9). All fields and coordinates are now dimensionless and no trace of the mass parameter m is left in the equations. However, one has to remember that the unity of length corresponds to the dimensionful $1/\mathrm{m}$, which is the physical length scale.

In what follows we shall be analyzing equations (2.18) without making any assumptions about values of κ_1, κ_2 and b_k. However, when integrating the equations numerically, we shall assume that $\kappa_1 + \kappa_2 = 1$ and choose b_k according to (2.15). Therefore, our solutions depend on three parameters of the theory, c_3, c_4 and η, where

$$\kappa_1 = \cos^2\eta, \qquad \kappa_2 = \sin^2\eta. \tag{2.20}$$

We shall assume in what follows that if the theory is extended to include an extra matter variables denoted by Ψ, then the action (2.1) becomes $S[\mathrm{g}, \mathrm{f}] \to S[\mathrm{g}, \mathrm{f}] + S_{\mathrm{mat}}[\mathrm{g}, \Psi]$, so that the matter couples only to the g metric. The g-geometry is therefore physically measurable as test particles follow its geodesics. The f-geometry is not directly coupled to matter, hence it cannot be directly seen and remains hidden.

III. SPHERICAL SYMMETRY

Let us introduce coordinates $(x^0, x^1, x^2, x^3) = (t, r, \vartheta, \varphi)$ and choose both metrics to be static, spherically symmetric, and diagonal,

$$ds^2_g = g_{\mu\nu}dx^\mu dx^\nu = -Q^2dt^2 + \frac{dr^2}{\Delta^2} + R^2d\Omega^2,$$
$$ds^2_f = f_{\mu\nu}dx^\mu dx^\nu = -q^2dt^2 + \frac{dr^2}{W^2} + U^2d\Omega^2, \tag{3.1}$$

where $d\Omega^2 = d\vartheta^2 + \sin^2\vartheta d\varphi^2$ while Q, Δ, R, q, W, U are functions of the radial coordinate $r = \mathrm{m}r$. In fact, this is not the most general form of the spherically symmetric fields, since one could also include the off-diagonal metric element f_{01} as shown by Eq. (B1) in Appendix B. However, in the *static* case this would imply that (1.1) is the only possible solution [18] (the situation changes in the time-dependent case). Therefore, we choose the static metrics to be both diagonal, which leads to nontrivial solutions.

The tensor $\gamma^{\mu}{}_{\nu}$ in (2.2) then reads

$$\gamma^{\mu}{}_{\nu} = \mathrm{diag}\left[\frac{q}{Q}, \frac{\Delta}{W}, \frac{U}{R}, \frac{U}{R}\right], \tag{3.2}$$

and one obtains from (2.7)

$$\begin{aligned} T^{\mu}{}_{\nu} &= \mathrm{diag}[T^0{}_0, T^1{}_1, T^2{}_2, T^2{}_2], \\ \mathcal{T}^{\mu}{}_{\nu} &= \mathrm{diag}[\mathcal{T}^0{}_0, \mathcal{T}^1{}_1, \mathcal{T}^2{}_2, \mathcal{T}^2{}_2], \end{aligned} \tag{3.3}$$

where

$$\begin{aligned} T^0{}_0 &= -\mathcal{P}_0 - \mathcal{P}_1\frac{\Delta}{W}, \\ T^1{}_1 &= -\mathcal{P}_0 - \mathcal{P}_1\frac{q}{Q}, \\ T^2{}_2 &= -\mathcal{D}_0 - \mathcal{D}_1\left(\frac{q}{Q} + \frac{\Delta}{W}\right) - \mathcal{D}_2\frac{q\Delta}{QW}, \\ \mathbf{u}^2\mathcal{T}^0{}_0 &= -\mathcal{P}_2 - \mathcal{P}_1\frac{W}{\Delta}, \\ \mathbf{u}^2\mathcal{T}^1{}_1 &= -\mathcal{P}_2 - \mathcal{P}_1\frac{Q}{q}, \\ \mathbf{u}\mathcal{T}^2{}_2 &= -\mathcal{D}_3 - \mathcal{D}_2\left(\frac{Q}{q} + \frac{W}{\Delta}\right) - \mathcal{D}_1\frac{QW}{q\Delta}. \end{aligned} \tag{3.4}$$

Here $\mathbf{u} = U/R$ and

$$\begin{aligned} \mathcal{P}_m &= b_m + 2b_{m+1}\mathbf{u} + b_{m+2}\mathbf{u}^2, \\ \mathcal{D}_m &= b_m + b_{m+1}\mathbf{u} \quad (m = 0, 1, 2). \end{aligned} \tag{3.5}$$

The independent field equations are

$$\begin{aligned} G^0_0(g) &= \kappa_1 T^0{}_0, \qquad G^1_1(g) = \kappa_1 T^1{}_1, \\ G^0_0(f) &= \kappa_2 \mathcal{T}^0{}_0, \qquad G^1_1(f) = \kappa_2 \mathcal{T}^1{}_1, \end{aligned} \tag{3.6}$$

plus the conservation condition $\overset{(g)}{\nabla}_{\mu} T^{\mu}_{\nu} = 0$, which has only one nontrivial component,

$$\overset{(g)}{\nabla}_{\mu} T^{\mu}{}_1 = (T^1{}_1)' + \frac{Q'}{Q}(T^1{}_1 - T^0{}_0) + 2\frac{R'}{R}(T^1{}_1 - T^2{}_2) = 0, \tag{3.7}$$

where the prime denotes differentiation with respect to r. The conservation condition for the second energy-momentum tensor also has only one nontrivial component,

$$\begin{aligned} \overset{(f)}{\nabla}_{\mu} \mathcal{T}^{\mu}{}_1 &= (\mathcal{T}^1{}_1)' + \frac{q'}{q}(\mathcal{T}^1{}_1 - \mathcal{T}^0{}_0) \\ &\quad + 2\frac{U'}{U}(\mathcal{T}^1{}_1 - \mathcal{T}^2{}_2) = 0, \end{aligned} \tag{3.8}$$

but this follows from (3.7) due to the identity relation (2.9). As a result, there are 5 independent equations in (3.6), (3.7), which is enough to determine the 6 field amplitudes Q, Δ, R, q, W, U, because the freedom of reparametrization of the radial coordinate $r \to \tilde{r}(r)$ allows one to fix one of the amplitudes.

IV. FIELD EQUATIONS

Let us introduce new functions

$$N = \Delta R', \qquad Y = WU', \tag{4.1}$$

in terms of which the two metrics read

$$\begin{aligned} ds_g^2 &= -Q^2 dt^2 + \frac{dR^2}{N^2} + R^2 d\Omega^2, \\ ds_f^2 &= -q^2 dt^2 + \frac{dU^2}{Y^2} + U^2 d\Omega^2. \end{aligned} \tag{4.2}$$

The advantage of this parametrization is that the second derivatives disappear from the Einstein tensor and the four Einstein equations (3.6) become

$$N' = -\frac{\kappa_1}{2}\frac{R}{NY}(R'Y\mathcal{P}_0 + U'N\mathcal{P}_1) + \frac{(1-N^2)R'}{2RN}, \tag{4.3}$$

$$Y' = -\frac{\kappa_2}{2}\frac{R^2}{UNY}(R'Y\mathcal{P}_1 + U'N\mathcal{P}_2) + \frac{(1-Y^2)U'}{2UY}, \tag{4.4}$$

$$Q' = -\left(\kappa_1(Q\mathcal{P}_0 + q\mathcal{P}_1) + \frac{Q(N^2-1)}{R^2}\right)\frac{RR'}{2N^2}, \tag{4.5}$$

$$q' = -\left(\kappa_2(Q\mathcal{P}_1 + q\mathcal{P}_2) + \frac{q(Y^2-1)}{R^2}\right)\frac{R^2U'}{2Y^2U}. \tag{4.6}$$

The conservation condition (3.7) reads

$$\begin{aligned} \overset{(g)}{\nabla}_{\mu} T^{\mu}{}_1 &= \frac{U'}{R}\left(1 - \frac{N}{Y}\right)\left(d\mathcal{P}_0 + \frac{q}{Q}d\mathcal{P}_1\right) \\ &\quad + \left(\frac{q'}{Q} - \frac{NQ'U'}{YQR'}\right)\mathcal{P}_1 = 0, \end{aligned} \tag{4.7}$$

and using Eqs. (4.5) and (4.6), this reduces to

$$R^2 Q \overset{(g)}{\nabla}_{\mu} T^{\mu}{}_1 = \frac{U'}{Y}\mathbf{C} = 0, \tag{4.8}$$

where

$$\mathbf{C} = \left(\kappa_2 \frac{R^4\mathcal{P}_1^2}{2UY} - \kappa_1 \frac{R^3\mathcal{P}_0\mathcal{P}_1}{2N} - \frac{(N^2-1)R\mathcal{P}_1}{2N} + (N-Y)Rd\mathcal{P}_0\right)Q + \left(\kappa_2 \frac{R^4\mathcal{P}_1\mathcal{P}_2}{2UY} - \kappa_1 \frac{R^3\mathcal{P}_1^2}{2N} + \frac{(Y^2-1)R^2\mathcal{P}_1}{2UY} + (N-Y)Rd\mathcal{P}_1\right)q, \tag{4.9}$$

with

$$d\mathcal{P}_m = 2(b_{m+1} + b_{m+2}\mathbf{u}) \quad (m = 0, 1). \tag{4.10}$$

The conservation condition (3.8) becomes

$$-U^2 q \overset{(f)}{\nabla}_\mu \mathcal{T}^\mu{}_1 = \frac{R'}{N}\mathbf{C} = 0. \tag{4.11}$$

The two conditions (4.8) and (4.11) will be fulfilled if $U' = R' = 0$, in which case both metrics are degenerate. If the metrics are not degenerate, then conditions (4.8) and (4.11) reduce to the algebraic constraint

$$\mathbf{C} = 0. \tag{4.12}$$

This constraint can be resolved with respect to q to give

$$q = \Sigma(R, U, N, Y)Q, \tag{4.13}$$

where $\Sigma(N, Y, R, U)$ is the (negative) ratio of the coefficients in front of Q and q in (4.9).

As a result, we obtain four differential equations (4.3)–(4.6) plus one algebraic constraint (4.12). The same equations can be obtained by inserting the metrics (4.2) directly to the action (2.1), which gives

$$S = \frac{4\pi}{\mathrm{m}^2\boldsymbol{\kappa}}\int L dt dr, \tag{4.14}$$

where, dropping a total derivative,

$$L = \frac{1}{\kappa_1}\left(\frac{(1-N^2)R'}{N} - 2RN'\right)Q + \frac{1}{\kappa_2}\left(\frac{(1-Y^2)U'}{Y} - 2UY'\right)q - \frac{QR^2R'}{N}\mathcal{P}_0 - \left(\frac{QR^2U'}{Y} + \frac{qR^2R'}{N}\right)\mathcal{P}_1 - \frac{qR^2U'}{Y}\mathcal{P}_2. \tag{4.15}$$

Varying L with respect to N, Y, Q, q gives Eqs. (4.3)–(4.6), while varying it with respect to R, U reproduces conditions (4.8) and (4.11). The equations and the Lagrangian L are invariant under the interchange symmetry (2.5), which now reads

$$\kappa_1 \leftrightarrow \kappa_2, \quad Q \leftrightarrow q, \quad N \leftrightarrow Y, \quad R \leftrightarrow U, \quad b_m \leftrightarrow b_{4-m}. \tag{4.16}$$

Equations (4.3)–(4.6) contain R' and U' which are not yet known. One of these two amplitudes can be fixed by imposing a gauge condition, but the other one should be determined dynamically. We need therefore one more condition, and the only way to get it is to differentiate the constraint. Since the constraint should be stable, this gives the secondary constraint:

$$\mathbf{C}' = \frac{\partial\mathbf{C}}{\partial N}N' + \frac{\partial\mathbf{C}}{\partial Y}Y' + \frac{\partial\mathbf{C}}{\partial Q}Q' + \frac{\partial\mathbf{C}}{\partial q}q' + \frac{\partial\mathbf{C}}{\partial R}R' + \frac{\partial\mathbf{C}}{\partial U}U' = 0. \tag{4.17}$$

Expressing here the derivatives N', Y', Q', q' by Eqs. (4.3)–(4.6) and using the relation (4.13), this condition reduces to

$$\mathbf{C}' = \mathcal{A}(R, U, N, Y)R' + \mathcal{B}(R, U, N, Y)U' = 0, \tag{4.18}$$

where the functions $\mathcal{A}(R, U, N, Y)$ and $\mathcal{B}(R, U, N, Y)$ are rather complicated and we do not show them explicitly. When the radial coordinate changes, both R' and U' change,

$$r \to \tilde{r}(r), \qquad R' \to \tilde{R}' = R'\frac{dr}{d\tilde{r}}, \qquad U' \to \tilde{U}' = U'\frac{dr}{d\tilde{r}}, \tag{4.19}$$

but the relation (4.18) between R' and U' remains the same. The secondary constraint can be resolved with respect to U',

$$U' = -\frac{\mathcal{A}(R, U, N, Y)}{\mathcal{B}(R, U, N, Y)}R' \equiv \mathcal{D}_U(R, U, N, Y)R'. \tag{4.20}$$

We can now use the gauge symmetry (4.19) to impose the coordinate condition

$$R' = 1 \Rightarrow R = r, \tag{4.21}$$

and then (4.20) reduces to

$$U' = \mathcal{D}_U(r, U, N, Y). \tag{4.22}$$

Now, U' appears in the right-hand sides of Eqs. (4.3) and (4.4), and replacing it there by the value (4.22), these two equations together with (4.22) form a closed system of three equations

$$N' = \mathcal{D}_N(r, U, N, Y),$$
$$Y' = \mathcal{D}_Y(r, U, N, Y),$$
$$U' = \mathcal{D}_U(r, U, N, Y). \tag{4.23}$$

The amplitudes Q, q are determined as follows. Injecting (4.13) to (4.5) yields the equation

$$Q' = -\frac{r}{2N^2}\left(\kappa_1(\mathcal{P}_0 + \Sigma(r, U, N, Y)\mathcal{P}_1) + \frac{N^2-1}{r^2}\right)Q \equiv \mathcal{F}(r, U, N, Y)Q, \tag{4.24}$$

which determines Q, and when its solution is known, q is determined algebraically from (4.13).

Solutions of (4.23), (4.24) and (4.13) are automatically compatible with (4.3)–(4.6) and with the constraint (4.12). For example, the algebraic solution for q given by (4.13) is compatible with its differential equation (4.6) because the latter contains U' not defined by (4.3)–(4.6). To determine U' one needs to differentiate the constraint (4.12) whose algebraic solution is (4.13) and to use (4.3)–(4.6). This completes the procedure in a consistent way.

In what follows we shall mainly focus on the three coupled equations (4.23) determining N, Y, U. As soon as their solution is obtained, the amplitudes Q, q are determined from (4.24) and (4.13).

V. ANALYTICAL SOLUTIONS

Some simple solutions of the equations can be obtained analytically [18,52], for which it is convenient to use the equations in the form (4.3)–(4.6).

A. Proportional backgrounds

Choosing the two metrics to be conformally related [18,52],

$$ds_f^2 = C^2 ds_g^2, \tag{5.1}$$

with a constant C, the solution is given by

$$Q^2 = N^2 = Y^2 = 1 - \frac{2M}{r} - \frac{\Lambda(C)}{3}r^2, \qquad R = r,$$
$$q = CQ, \qquad U = CR, \tag{5.2}$$

which describes two proportional Schwarzschild–(anti-)de Sitter geometries. The constant C and the cosmological constant $\Lambda(C)$ are determined by

$$\kappa_1(\mathcal{P}_0 + C\mathcal{P}_1) = \frac{\kappa_2}{C}(\mathcal{P}_1 + C\mathcal{P}_2) \equiv \Lambda(C). \tag{5.3}$$

Since $\mathcal{P}_m$ defined by (3.5) are polynomials in $\mathbf{u} = U/R = C$, this yields an algebraic equation for C that can have up to four real roots. If the parameters b_k are chosen according to (2.15), then one of the roots is $C = 1$, in which case $\Lambda = 0$.

The value of the dimensionful cosmological constant $\mathbf{\Lambda}$ should agree with the observation, hence one should have

$$\mathbf{\Lambda} = \mathrm{m}^2\Lambda \sim 1/R_{\mathrm{Hub}}^2 \tag{5.4}$$

where R_{Hub} is the Hubble radius of our Universe. One way to fulfill this relation is to assume that the graviton mass is extremely small such that the Compton length is of the order of the Hubble radius,

$$1/\mathrm{m} \sim R_{\mathrm{Hub}}. \tag{5.5}$$

However, the relation can also be fulfilled by assuming that Λ is very small, which is possible if there is a hierarchy between the two couplings: $\kappa_1 \ll \kappa_2 = 1 - \kappa_1 \sim 1$. Equation (5.3) implies then that $\Lambda \sim \kappa_1$ and that C should be very close to a root of $\mathcal{P}_1 + C\mathcal{P}_2$. The hierarchy between the two couplings is in fact necessary to reconcile with the observations the perturbation spectrum of the massive bigravity cosmology, because it contains an instability in the scalar sector [53–55]. For this one should assume that [13–17]

$$\frac{\kappa_1}{\kappa_2} \approx \kappa_1 \le \left(\frac{\mathrm{M_{ew}}}{\mathrm{M_{Pl}}}\right)^2 \sim 10^{-34} \ll 1, \tag{5.6}$$

where $\mathrm{M_{ew}} \sim 100$ GeV is the electroweak energy scale and $\mathrm{M_{Pl}} \sim 10^{19}$ GeV is the Planck mass. Here 10^{-34} is the *upper bound* for κ_1 imposing which shifts the instability toward early times making it unobservable. However, κ_1 can also be less then this bound [13], hence

$$\kappa_1 = \gamma^2 \times 10^{-34} \quad \text{with} \quad \gamma \in [0, 1]. \tag{5.7}$$

As a result,

$$1/\mathrm{m} \sim \sqrt{\Lambda}R_{\mathrm{Hub}} = \sqrt{\kappa_1}R_{\mathrm{Hub}} = \gamma \times \left(\frac{\mathrm{M_{ew}}}{\mathrm{M_{Pl}}}\right)R_{\mathrm{Hub}} \sim \gamma \times 10^6 \text{ km}, \tag{5.8}$$

which is of the order of the solar size if $\gamma \sim 1$. However, in what follows we shall not be always assuming κ_1 to be small and shall present our results for arbitrary $\kappa_1 \in [0, 1]$.

B. Deformed AdS background

Choosing U, q to be constant,

$$U = U_0, \qquad q = q_0, \tag{5.9}$$

solves Eqs. (4.6) and (4.8), while Eqs. (4.3)–(4.5) then can be integrated in quadratures [18]. However, such solution is unacceptable, since the f metric degenerates if $U' = 0$. At the same time, there are other, more general solutions

which approach (5.9) for $r \to \infty$, and for these solutions U' vanishes only asymptotically, hence they are acceptable. The leading at large r terms of such solutions are

$$N^2 = -\kappa_1 \frac{b_0}{3} r^2 - \kappa_1 b_1 U_0 r + \mathcal{O}(1),$$
$$Y = -\frac{\sqrt{3}\kappa_2 b_1}{4U_0\sqrt{-\kappa_1 b_0}} r^2 + \mathcal{O}(r),$$
$$Q = \frac{q_0}{4U_0} r + \mathcal{O}(1), \qquad U = U_0 + \mathcal{O}\left(\frac{1}{r}\right),$$
$$q = q_0 + \mathcal{O}\left(\frac{1}{r}\right). \tag{5.10}$$

The g metric approaches the AdS metric in the leading $\mathcal{O}(r^2)$ order, but the subleading terms do not have the AdS structure.

It turns out that solutions of Eqs. (4.3)–(4.6) generically approach for $r \to \infty$ either (5.2) or (5.10) (or they show a curvature singularity at a finite r), hence they are not asymptotically flat [18].

VI. BOUNDARY CONDITIONS AT THE HORIZON

Let us require the g metric to have a regular event horizon at some $r = r_H$ by demanding the metric components $g_{00} = Q^2$ and $g^{rr} = N^2$ to show simple zeroes at this point. Therefore, we demand that close to this point one has $Q^2 \sim N^2 \sim r - r_H$ and we consider only the exterior region $r \geq r_H$ where $Q^2 > 0$ and $N^2 > 0$. Such a behavior is compatible with the field equations if only the f metric also shows a regular horizon at the same place, hence $q^2 \sim Y^2 \sim r - r_H$. As a result, both metrics share a horizon at the same place $r = r_H$, in agreement with [37,38]. However, the horizon radius measured by the g metric, r_H, can be different from the radius measured by the second metric, $U(r_H)$. We therefore introduce the parameter $u \equiv \mathbf{u}(r_H) = U(r_H)/r_H$.

As a result, the local solutions close to the horizon are expected to have the form

$$N^2 = \sum_{n\geq 1} a_n (r - r_H)^n, \qquad Y^2 = \sum_{n\geq 1} b_n (r - r_H)^n,$$
$$U = u r_H + \sum_{n\geq 1} c_n (r - r_H)^n, \tag{6.1}$$

the two other amplitudes being

$$Q^2 = \sum_{n\geq 1} d_n (r - r_H), \qquad q^2 = \sum_{n\geq 1} e_n (r - r_H)^n. \tag{6.2}$$

The equations then allow one to recurrently determine the coefficients a_n, b_n, c_n, d_n, e_n. It turns out they all can be expressed in terms of a_1, which should fulfil a quadratic equation

$$\mathcal{A} a_1^2 + \mathcal{B} a_1 + \mathcal{C} = 0 \Rightarrow a_1 = \frac{1}{2\mathcal{A}}(-\mathcal{B} + \sigma\sqrt{\mathcal{B}^2 - 4\mathcal{A}\mathcal{C}}),$$
$$\sigma = \pm 1, \tag{6.3}$$

where $\mathcal{A}$, B, C are functions of u, r_H and of the theory parameters b_k, κ_1, κ_2. It turns out that one should choose $\sigma = +1$, since choosing $\sigma = -1$ always yields singular solutions. Therefore, for a chosen a value of the horizon size r_H, the local solutions (6.1), (6.2) comprise a set labeled by a continuous parameter u. These local solutions determine the boundary conditions at the horizon, and they can be numerically extended to the region $r > r_H$.

The surface gravity for each metric is [18]

$$\kappa_g^2 = \lim_{r\to r_H} Q^2 N'^2 = \frac{1}{4} d_1 a_1, \quad \kappa_f^2 = \lim_{r\to r_H} q^2 \left(\frac{Y}{U'}\right)'^2 = \frac{e_1 b_1}{4c_1^2}, \tag{6.4}$$

and using the values of the expansion coefficients determined by the equations yields the relation $\kappa_g = \kappa_f$, hence the two surface gravities coincide, as coincide the Hawking temperatures,

$$T = \frac{\kappa_g}{2\pi} = \frac{\kappa_f}{2\pi}. \tag{6.5}$$

One has close to the horizon $N(r) \sim Y(r) \sim \sqrt{r - r_H}$ hence the derivatives N' and Y' are not defined at the horizon. The usual practice would then be to start the numerical integration not at $r = r_H$ but at a nearby point $r = r_H + \epsilon$. However, although the dependence on ϵ is expected to be small, still its presence in the procedure may lead to numerical instabilities. This point was emphasized in [45]. This difficulty can be resolved as follows. Setting

$$N(r) = S(r)\nu(r), \qquad Y(r) = S(r)y(r) \quad \text{with}$$
$$S(r) = \sqrt{1 - \frac{r_H}{r}}, \tag{6.6}$$

the functions $\nu(r)$, $y(r)$ and all their derivatives assume finite values at $r = r_H$. Making this change of variables in (4.23) gives a "desingularized" version of the equations that allows us to start the numerical integration exactly at $r = r_H$. This form of the equations is described in Appendix A.

To recapitulate, all black holes for a given r_H can be labeled by only one parameter u. If $u = 1$ then the two metrics coincide everywhere and the solution is Schwarzschild (1.2). If $u = C$ where C is a root of the algebraic equation (5.3), then the solutions is Schwarzschild–(anti-)de Sitter and is described by (5.1) and (5.2). For other values of u the numerical integration produces more general solutions which describe hairy black holes and which can be of the following

three qualitative types, depending on their asymptotic behavior [18].

(a) Solutions extending up to arbitrarily large values of r and asymptotically approaching a proportional AdS background (5.1), (5.2). At large r one has $N = N_0(1+\delta N)$, $Y = Y_0(1+\delta Y)$, $U = U_0(1+\delta U)$ where N_0, Y_0, U_0 are given by (5.2), while the deviations $\delta N, \delta Y, \delta U$ approach zero. In the linear approximation, the latter are described by

$$\delta N = \frac{A}{r^3}, \quad \delta U = B_1 e^{\lambda_1 r} + B_2 e^{\lambda_2 r}, \quad \delta Y = \mathcal{O}(\delta U), \tag{6.7}$$

where A, B_1, B_2 are integration constants and real parts of λ_1 and λ_2 are *negative*. All of these three perturbation modes vanish for $r \to \infty$, and since the number of equations (4.23) is also three, it follows that the AdS background is an *attractor* at large r.

(b) Solutions extending up to arbitrarily large values of r and asymptotically approaching a deformed AdS background (5.10). The latter is also an attractor at large r.

(c) Solutions extending only up to $r = r_s < \infty$ where derivatives of some metric functions diverge, which corresponds to a curvature singularity.

This exhausts the possible types of *generic* solutions. If one integrates the equation for many different values of u, one always obtains solutions of the above three types and one does not find asymptotically flat solutions other than Schwarzschild. For example, choosing $u = 1 + \epsilon$ yields solutions which are almost Schwarzschild in a region close to the horizon, but for larger values of r they deviate from the Schwarzschild metric more and more [18] (this means the Schwarzschild solution is Lyapunov unstable [45]). All of this does not mean that the Schwarzschild is the only asymptotically flat black hole solution. There may be others, but they are not parametrically close to the Schwarzschild solution and should correspond to some discrete values of u which are difficult to detect by a "brute force" method.

VII. BOUNDARY CONDITIONS AT INFINITY

Let us suppose the solutions to approach flat space with $g_{\mu\nu} = f_{\mu\nu} = \eta_{\mu\nu}$ at large r and set

$$N = 1 + \delta N, \qquad Y = 1 + \delta Y, \qquad U = r + \delta U. \tag{7.1}$$

In fact, a more general possibility would be to require the g metric to approach the flat Minkowski metric $\mathrm{diag}(-1,1,1,1)$ and the f metric to approach just a flat metric, as for example $\mathrm{diag}(-a^2, b^2, b^2, b^2)$ with constat a, b. This would lead to solutions whose Lorentz invariance is broken in the asymptotic region [27,28]. However, we shall not analyze this option.

Inserting (7.1) to (4.23) yields

$$\begin{aligned}
\delta N' &= -\frac{1}{r}(\kappa_2 \delta N + \kappa_1 \delta Y) - \kappa_1 \delta U + \mathcal{N}_N, \\
\delta Y' &= -\frac{1}{r}(\kappa_2 \delta N + \kappa_1 \delta Y) + \kappa_2 \delta U + \mathcal{N}_Y, \\
\delta U' &= \left(1 + \frac{2}{r^2}\right)(\delta Y - \delta N) + \mathcal{N}_U,
\end{aligned} \tag{7.2}$$

where $\mathcal{N}_N, \mathcal{N}_Y, \mathcal{N}_U$ are the nonlinear in $\delta N, \delta Y, \delta U$ parts of the right-hand sides $\mathcal{D}_N$, $\mathcal{D}_Y$, $\mathcal{D}_U$ in (4.23). Neglecting the nonlinear terms, the solution of these equations is

$$\begin{aligned}
\delta N &= \frac{A}{r} + B\kappa_1 \frac{1+r}{r} e^{-r} + C\kappa_1 \frac{1-r}{r} e^{+r}, \\
\delta Y &= \frac{A}{r} - B\kappa_2 \frac{1+r}{r} e^{-r} - C\kappa_2 \frac{1-r}{r} e^{+r}, \\
\delta U &= B\frac{r^2+r+1}{r^2} e^{-r} + C\frac{r^2-r+1}{r^2} e^{+r},
\end{aligned} \tag{7.3}$$

where A, B, C are integration constants. The part of this solution proportional to A is the Newtonian mode describing the massless graviton subject to the linearized Einstein equations (2.11). The other two modes proportional to B and C fulfill the Fierz-Pauli equations (2.12) and describe the massive graviton, hence they contain the Yukawa exponents (remember that $r = \mathrm{mr}$).

As one can see, among the three modes only two are stable for $r \to \infty$ while the third one diverges in this limit, hence *flat space is not an attractor*. This is why one cannot get asymptotically flat solutions by simply integrating from the horizon—trying to approach flat space in this way, the unstable mode e^{+r} rapidly wins and drives the solution away from flat space. The only way to proceed is to suppress the unstable mode from the very beginning by requiring the solution at large r to be

$$\begin{aligned}
\delta N &= \frac{A}{r} + B\kappa_1 \frac{1+r}{r} e^{-r} + \ldots, \\
\delta Y &= \frac{A}{r} - B\kappa_2 \frac{1+r}{r} e^{-r} + \ldots, \\
\delta U &= r + B\frac{r^2+r+1}{r^2} e^{-r} + \ldots,
\end{aligned} \tag{7.4}$$

where the dots denote nonlinear corrections. The usual practice would be to neglect the dots and assume that the linear terms approximate the solution everywhere for $r > r_\star$, where $r_\star$ is some large value. However, one can check that already the quadratic correction contains an additional factor of $\ln(r)$ and hence dominates the linear part for $r \to \infty$. Therefore, nonlinear corrections are important, but if all of them are taken into account, it is not obvious that the solution will remain asymptotically flat.

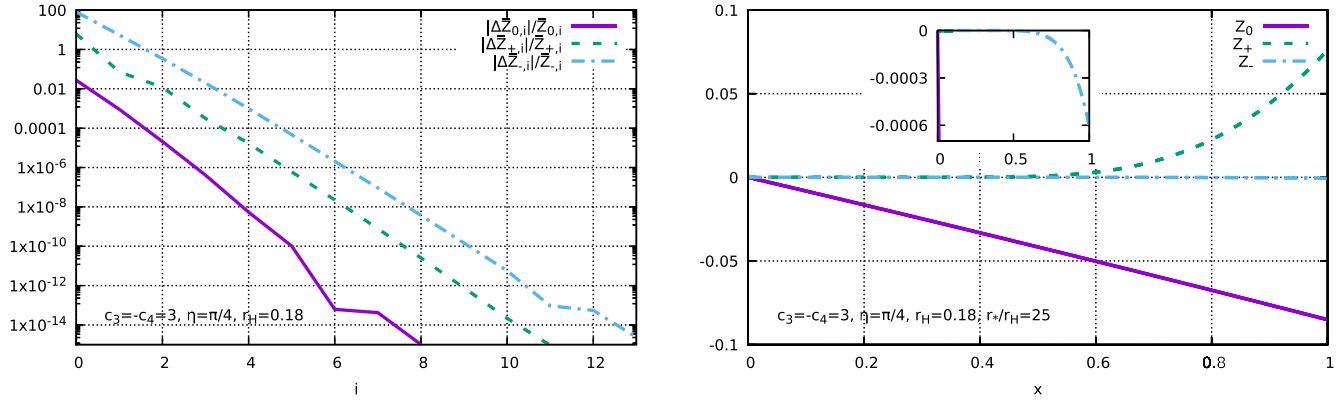

FIG. 1. Left: convergence of the iterations of the integral equations (7.8). Right: the amplitudes Z_0, $Z_\pm$ against $x = r_\star/r$, where the insertion shows a closeup of Z_-.

Fortunately, problems of this kind have been studied—see, e.g., [47]. To take the nonlinear corrections into account, the procedure is as follows. Let us express $\delta N, \delta Y, \delta U$ in terms of three functions Z_0, Z_+, Z_-:

$$\delta N = Z_0 + \kappa_1 \frac{1+r}{r} Z_+ + \kappa_1 \frac{1-r}{r} Z_-,$$
$$\delta Y = Z_0 - \kappa_2 \frac{1+r}{r} Z_+ - \kappa_2 \frac{1-r}{r} Z_-,$$
$$\delta U = \frac{1+r+r^2}{r^2} Z_+ + \frac{1-r+r^2}{r^2} Z_-. \tag{7.5}$$

Equations (7.2) then assume the form

$$Z_0' + \frac{Z_0}{r} = \mathcal{S}_0(r, Z_0, Z_\pm) \equiv \kappa_1 \mathcal{N}_Y + \kappa_2 \mathcal{N}_N,$$
$$Z_+' + Z_+ = \mathcal{S}_+(r, Z_0, Z_\pm) \equiv \frac{r^2 - r + 1}{2r^2}(\mathcal{N}_N - \mathcal{N}_Y) + \frac{r-1}{2r}\mathcal{N}_U,$$
$$Z_-' - Z_- = \mathcal{S}_-(r, Z_0, Z_\pm) \equiv \frac{r^2 + r + 1}{2r^2}(\mathcal{N}_Y - \mathcal{N}_N) + \frac{r+1}{2r}\mathcal{N}_U. \tag{7.6}$$

Terms on the left in these equations are linear in $Z_0, Z_\pm$, while those on the right are nonlinear. Neglecting the nonlinear terms, the solution is $Z_0 = 1/r$, $Z_+ = e^{-r}$, $Z_- = e^{+r}$, and if we set

$$Z_0 = \frac{A}{r}, \qquad Z_+ = Be^{-r}, \qquad Z_- = 0, \tag{7.7}$$

this reproduces the linear part of (7.4). Now, to take the nonlinear terms into account, one converts Eqs. (7.6) into the equivalent set of integral equations,

$$Z_0(r) = \frac{A}{r} - \int_r^\infty \frac{\bar{r}}{r} \mathcal{S}_0(\bar{r}, Z_0(\bar{r}), Z_\pm(\bar{r}))d\bar{r},$$
$$Z_+(r) = Be^{-r} + \int_{r_\star}^r e^{\bar{r}-r} \mathcal{S}_+(\bar{r}, Z_0(\bar{r}), Z_\pm(\bar{r}))d\bar{r},$$
$$Z_-(r) = -\int_r^\infty e^{r-\bar{r}} \mathcal{S}_-(\bar{r}, Z_0(\bar{r}), Z_\pm(\bar{r}))d\bar{r}, \tag{7.8}$$

where $r_\star$ is some large value. These equations determine the solution for $r > r_\star$, and they are solved by iterations. To start the iterations, one neglects the nonlinear terms, which gives the configuration (7.7). The next step is to inject this configuration to the integrals, which gives the corrected configuration, and so on. In practice, one introduces variables $x = r_\star/r$ and $\bar{x} = r_\star/\bar{r}$ assuming values in the interval [0, 1], and then one discretizes the interval to compute the integrals.

To see the convergence of the iterations, we compute for each Z and for each discretization point the difference $\Delta Z_i = Z_{i+1} - Z_i$ of the results of the consecutive $(i+1)$th and ith iterations, and then we take the average $\overline{\Delta Z_i}$ over all discretization points. Computing similarly the average $\bar{Z}_i$ of Z_i, the ratios $\overline{\Delta Z_i}/\bar{Z}_i$ decrease with i exponentially fast, as seen on the left panel in Fig. 1, hence the iterations converge. The solution of the integral equations is shown on the right panel in Fig. 1: the amplitudes Z_0 and $Z_\pm$ against $x = r_\star/r$ (for $r_\star = 25 r_H$). One can see that the amplitude Z_- is always small but nonvanishing, and that all the three amplitudes vanish for $x = 0$, hence the solution is indeed asymptotically flat.

This yields an asymptotically flat solution in the region $r > r_\star$. To extend this solution to the region $r_H < r < r_\star$ one only needs its values at $r = r_\star$,

$$Z_0(r_\star) = \frac{A}{r_\star} - \int_{r_\star}^\infty \frac{\bar{r}}{r} \mathcal{S}_0(\bar{r}, Z_0(\bar{r}), Z_\pm(\bar{r}))d\bar{r},$$
$$Z_+(r_\star) = Be^{-r_\star},$$
$$Z_-(r_\star) = -\int_{r_\star}^\infty e^{r_\star - \bar{r}} \mathcal{S}_-(\bar{r}, Z_0, Z_\pm)d\bar{r}. \tag{7.9}$$

To recapitulate, the described above procedure yields the boundary values for the fields at a large $r_\star$ and makes sure that the solution for $r > r_\star$ exists and is indeed asymptotically flat. It is worth noting that the parameter A determines the Arnowitt-Deser-Misner (ADM) mass,

$$M = -A. \tag{7.10}$$

VIII. NUMERICAL PROCEDURE

Summarizing the above discussion, the asymptotically flat black holes are described by solutions of the three coupled first order ODEs (4.23) for the three functions $N(r)$, $Y(r)$, $U(r)$ [which determines also $Q(r)$, $q(r)$] with the following boundary conditions. At the horizon $r = r_H$ one has

$$N(r) = \sqrt{1-\frac{r_H}{r}}\,\nu(r), \qquad Y(r) = \sqrt{1-\frac{r_H}{r}}\,y(r), \tag{8.1}$$

where the horizon values $\nu(r_H) \equiv \nu_H$ and $y(r_H) \equiv y_H$ are finite and determined by the Eqs. (A8), (A6) in Appendix A, while $U(r_H) \equiv U_H \equiv ur_H$ can be arbitrary. Therefore, all possible boundary conditions at the horizon are labeled by just one free parameter u, and choosing some value for it, the equations can be integrated directly from the horizon, as explained in Appendix A, to the outer region $r > r_H$.

Far from the horizon, at $r = r_\star \gg r_H$, one has

$$\begin{aligned}
N(r_\star) &= 1 + Z_0(r_\star) + \kappa_1 B\frac{1+r_\star}{r_\star}e^{-r_\star} + \kappa_1\frac{1-r_\star}{r_\star}Z_-(r_\star),\\
Y(r_\star) &= 1 + Z_0(r_\star) - \kappa_2 B\frac{1+r_\star}{r_\star}e^{-r_\star} - \kappa_2\frac{1-r_\star}{r_\star}Z_-(r_\star),\\
U(r_\star) &= r_\star + B\frac{1+r_\star+r_\star^2}{r_\star^2}e^{-r_\star} + \frac{1-r_\star+r_\star^2}{r_\star^2}Z_-(r_\star),
\end{aligned} \tag{8.2}$$

where $Z_0(r_\star)$ and $Z_-(r_\star)$ are functions of A, B determined by (7.9) via iterating the integral equations (7.8).

As a result, we have the boundary conditions at $r = r_H$ labeled by u and the boundary conditions at $r = r_\star$ labeled by A, B. We use them to construct solutions in the region $r_H \le r \le r_\star$. To this end, we choose some value of u and integrate numerically the equations starting from $r = r_H$ as far as some $r = r_0 < r_\star$ and we obtain at this point some values which will depend on r_H and u:

$$\begin{aligned}
&N(r_0) \equiv N_{\rm hor}(r_H, u), \qquad Y(r_0) \equiv Y_{\rm hor}(r_H, u),\\
&U(r_0) \equiv U_{\rm hor}(r_H, u).
\end{aligned} \tag{8.3}$$

Then we choose A, B and numerically extend the large r data (8.2) from $r = r_\star$ down to $r = r_0$, thereby obtaining

$$\begin{aligned}
&N(r_0) \equiv N_{\rm inf}(A, B), \qquad Y(r_0) \equiv Y_{\rm inf}(A, B),\\
&U(r_0) \equiv U_{\rm inf}(A, B).
\end{aligned} \tag{8.4}$$

If the two sets of values agree, hence if

$$\begin{aligned}
\Delta N(r_H, u, A, B) &\equiv N_{\rm hor}(r_H, u) - N_{\rm inf}(A, B) = 0,\\
\Delta Y(r_H, u, A, B) &\equiv Y_{\rm hor}(r_H, u) - Y_{\rm inf}(A, B) = 0,\\
\Delta U(r_H, u, A, B) &\equiv U_{\rm hor}(r_H, u) - U_{\rm inf}(A, B) = 0,
\end{aligned} \tag{8.5}$$

then the solution in the interval $r \in [r_H, r_0]$ merges smoothly with the solution in the interval $r \in [r_0, r_\star]$ to represent one single solution in the interval $r \in [r_H, r_\star]$. The extension to the region $r > r_\star$ is then provided by the integral equations (7.8), finally yielding an asymptotically flat black hole solution in the region $r \in [r_H, \infty)$. It is worth noting that these solutions will depend neither on r_0 nor on $r_\star$; these values could be varied without affecting the global solution (which is a good consistency check).

In some cases using just two zones $[r_H, r_0]$ and $[r_0, r_\star]$ produces too large numerical errors. To keep the numerical instability under control, one should then integrate through many smaller zones $[r_H, r_0]$, $[r_0, r_1], [r_1, r_2] \ldots [r_k, r_\star]$ and perform matchings at $r_0, r_1, \ldots r_k$ (see Sec. 7.3.5 in [56]). This yields numerically stable results.

In the case of just two zones, the problem reduces to solving the matching conditions (8.5) by adjusting the values u, A, B. At least one solution to these three conditions certainly exists and corresponds to the Schwarzschild solution, for which

$$u = 1, \qquad A = -\frac{r_H}{2}, \qquad B = 0. \tag{8.6}$$

Are there other solutions? Since there are three matching conditions for the three variables, their solutions must constitute a *discrete* set of points (u_k, A_k, B_k) in the 3-space spanned by u, A, B. This implies that different black hole solutions with the same r_H are *parametrically isolated* from each other. This creates a problem, since in order to solve numerically algebraic equations (8.5), an input configuration u, A, B is needed to start the numerical iterations within the Newton-Raphson procedure [39]. However, unless the input configuration is close to the solution, the numerical iterations do not converge, hence some additional information is necessary to specify where to start the iterations.

As explained in the Introduction, the additional information is provided by the stability analysis of the Schwarzschild solution (1.2) [33,42]. In this analysis one considers the two metrics of the form (4.2) with

$$\begin{aligned}
&Q = S + \delta Q, \qquad N = S + \delta N, \qquad R = r\\
&q = S + \delta q, \qquad Y = S + \delta Y, \qquad U = r + \delta U,\\
&f_{01} = \delta\alpha,
\end{aligned} \tag{8.7}$$

where $S=\sqrt{1-\frac{r_H}{r}}$ while the perturbations $\delta Q, \delta N, \delta q, \delta Y, \delta U, \delta\alpha$ are assumed to be small and depend on t, r. It turns out that at the GL point, for $r_H=0.86$, the perturbation equations admit a *static* solution (zero mode) for which $\delta Q, \delta N, \delta q, \delta Y, \delta U$ depend only on r and are bounded everywhere in the region $r \geq r_H$ while $\delta\alpha=0$. This solution can be viewed as a perturbative approximation of a new solution that merges with the Schwarzschild solution for $r_H=0.86$.

This suggests that to get new solutions of the matching conditions (8.5), one should choose the event horizon size to be close $r_H=0.86$ and choose the input configuration u, A, B to be close to (8.6). Then the numerical iterations should converge to values u, A, B which are slightly different from (8.6) and correspond to an almost Schwarzschild black hole slightly distorted by a massive hair. Changing then iteratively the value of r_H yields solutions which deviate considerably from the Schwarzschild metric close to the horizon, but always approach flat metric in the asymptotic region.

IX. ASYMPTOTICALLY FLAT HAIRY BLACK HOLES

Applying the procedure outlined above, we were able to construct asymptotically flat hairy solutions. We confirm the results of Ref. [44] and obtain many new results.

First of all, we find that for r_H approaching from below the GL value, $r_H \approx 0.86$, there are asymptotically flat hairy black hole solutions for any c_3, c_4, η. They are very close to the Schwarzschild solution: one has $u=U_H/r_H \approx 1$ and the ADM mass $M \approx r_H/2$. However, for smaller values of r_H the solutions deviate more and more from Schwarzschild. To illustrate this, we plot in Fig. 2 the functions N/S, Q/S, Y/S, q/S, and U'. If these functions all equal to one, then the solution is Schwarzschild. As one can see, they indeed approach unity far away from the horizon, but close to the horizon they deviate considerably from unity, hence the massive graviton hair is concentrated in this region.

Solutions are regular for r_H close to 0.86; however, for smaller r_H and depending on values of c_3, c_4, η, the amplitudes Y, q, U' may show additional zeros outside the horizon, whereas Q, N always remain positive. This implies that the f metric is singular, because the invariants of its Riemann tensor diverge where the zeros are located. An example of this is shown on the lower two panels in Fig. 2, and also on the lower two panels in Fig. 3 where one can see that the phenomenon occurs when η approaches $\pi/2$. The fact that the f metric becomes singular does not invalidate the solutions because the f-geometry is not directly measurable and its singularities are not seen, while the g metric, which can be probed by test particles, remains

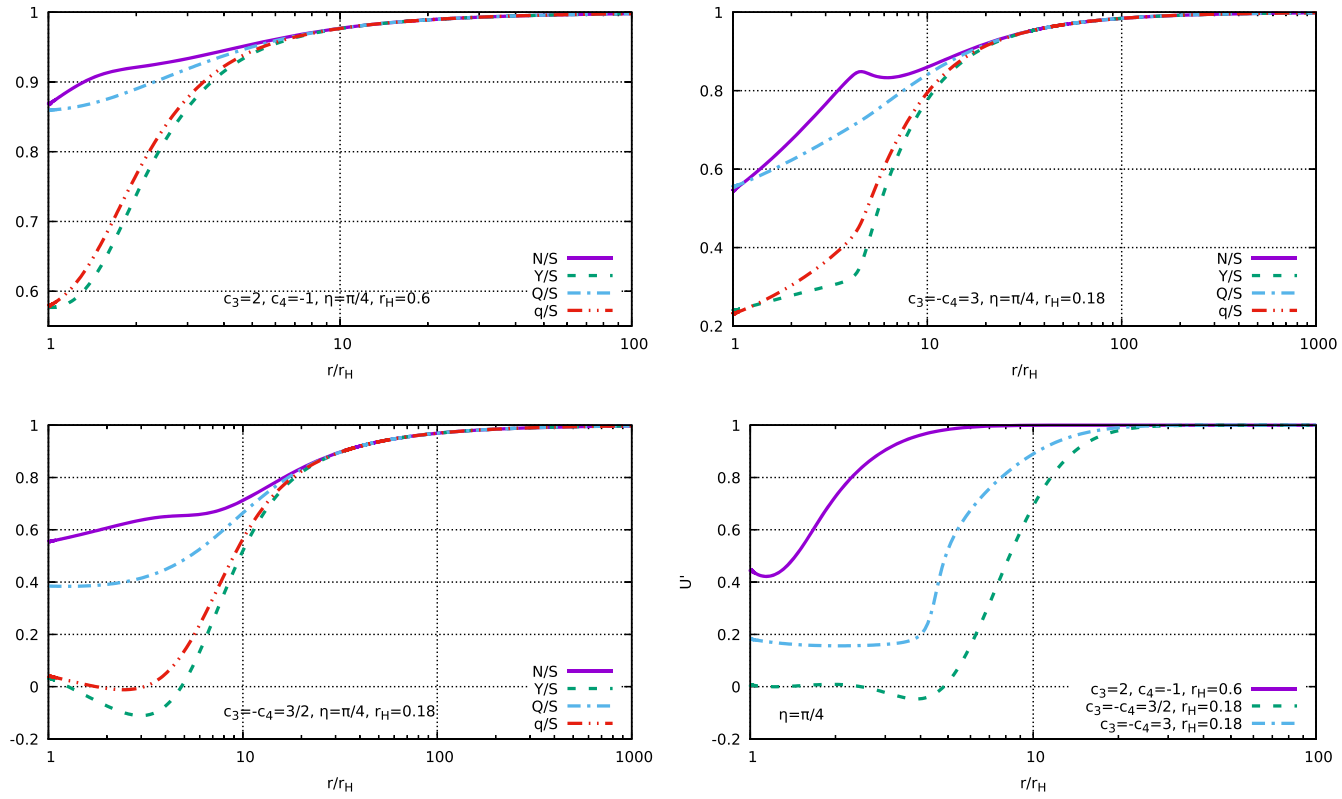

FIG. 2. Profiles of N/S, Y/S, Q/S, q/S with $S=\sqrt{1-r_H/r}$ and that of U' for solutions with $\eta=\pi/4$ but for various values of r_H, c_3, c_4. Solution with $c_3=-c_4=3/2$ shown on the two lower panels is singular because the amplitudes q, Y, U' develop zeros outside the horizon.

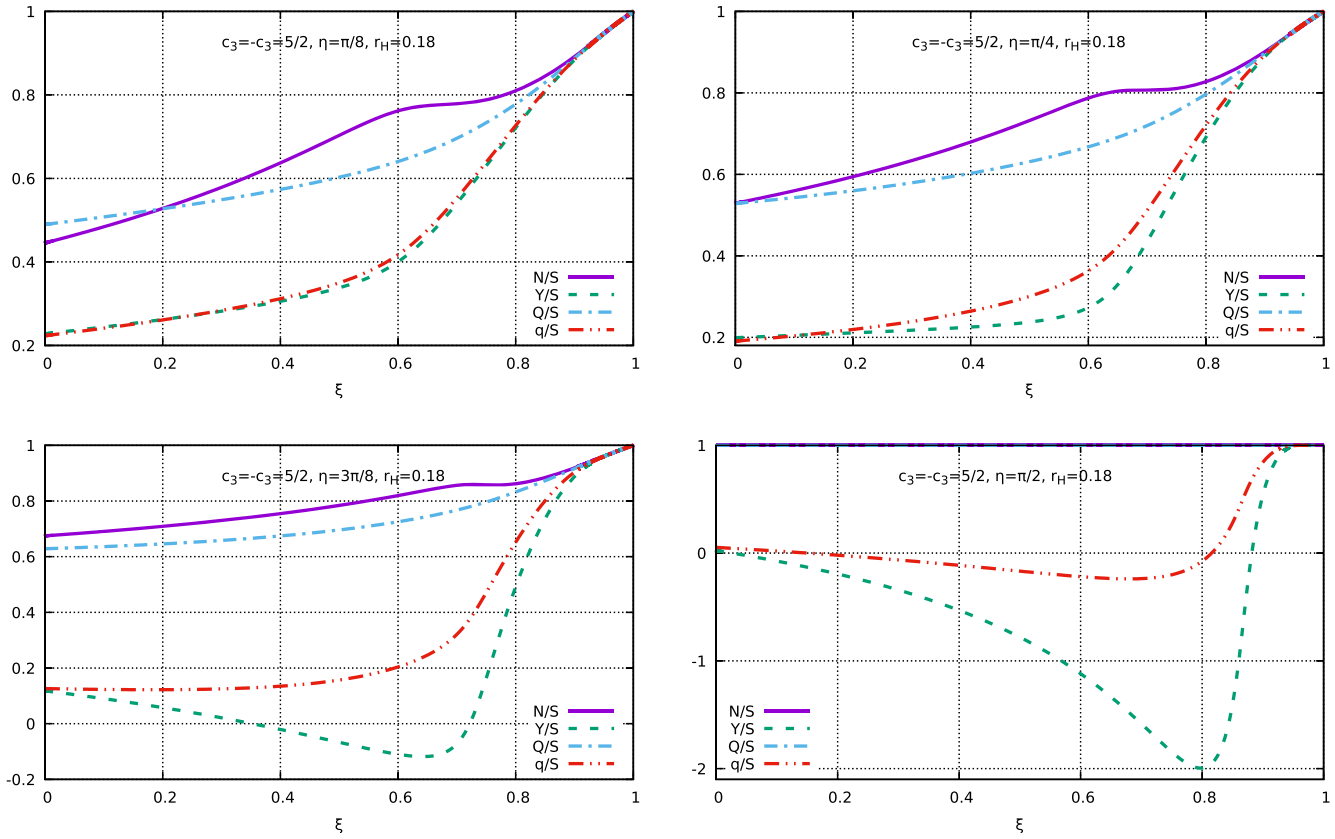

FIG. 3. Profiles of $N/S, Y/S, Q/S, q/S$ with $S = \sqrt{1 - r_H/r}$ against $\xi = (r - r_H)/(r + r_H)$ for solutions with the same c_3, c_4, r_H but for different values of η. When η approaches $\pi/2$ then the amplitudes Y, q start showing zeroes. For $\eta = \pi/2$ the g metric is Schwarzschild with $N/S = Q/S = 1$.

always regular. We shall therefore keep such solutions in our consideration.

Solutions in Fig. 2 are shown up to large but still finite values of the radial coordinate, $r/r_H \leq 100$ or $r/r_H \leq 1000$. What is shown is the combination of the solutions of differential equations (4.23) in the region $r_H \leq r \leq r_\star$ and of the integral equations (7.8) for $r > r_\star$ where $r_\star/r_H = 25$. At the same time, our procedure yields solutions in the whole region $r \in [r_H, \infty)$. Introducing the compactified radial variable

$$\xi = \frac{r - r_H}{r + r_H} \in [0, 1], \tag{9.1}$$

we plot in Fig. 3 the amplitudes N, Y, Q, q against ξ. As seen, the amplitudes approach unity as $\xi \to 1$ (same is true for U') hence the solutions are indeed asymptotically flat. The disadvantage of this parametrization is that the slope of the functions does not vanish for $\xi \to 1$. Indeed, for large r one has $N = 1 - M/r + \cdots$ and $\xi = 1 - r_H/r + \cdots$ hence at infinity $dN/d\xi = M/r_H$.

If $\eta = \pi/2$ then $\kappa_1 = 0$ and the g metric becomes Schwarzschild. The theory reduces then to the massive gravity for the dynamical f metric on a fixed Schwarzschild background. The solution for the f metric is shown on the lower right panel in Fig. 3. Similarly, for $\eta = 0$ one has $\kappa_2 = 0$ and the f metric is Schwarzschild, while the g metric is a solution of the massive gravity on the Schwarzschild background shown on the upper left panel in Fig. 4. One should emphasize that the radii of the background Schwarzschild black holes for $\eta = 0$ and for $\eta = \pi/2$ are not the same. For example, for $\eta = \pi/2$ the Schwarzschild black hole has $r_H = 0.18$ for the solution shown in Fig. 3, while for $\eta = 0$ the event horizon size is determined not by r_H but by $U_H = ur_H$ where $u \approx 5$ (as seen in Fig. 4) hence this time the Schwarzschild black hole is much larger. As a result, solutions on these different backgrounds look quite different—the solution for the f metric on the lower right panel in Fig. 3 shows zeros hence it is singular, while the solution for the g metric on the upper left panel in Fig. 4 is regular.

Solutions for $\eta = \pi/2$ will play an important role below. We shall call them "hairy Schwarzschild" because their g metric is Schwarzschild but their f metric supports hair.

Figure 4 shows the η dependence of $u = U_H/r_H$ and of the ADM mass M expressed in units of the Schwarzschild mass $M_S = r_H/2$, as well as the temperature T expressed in units of the Schwarzschild temperature $T_S = 1/(4\pi r_H)$. As one can see, the dependence is rather strong for small r_H, in particular for u. The decrease of the mass M with η can be understood by noting that the mass is the same with respect

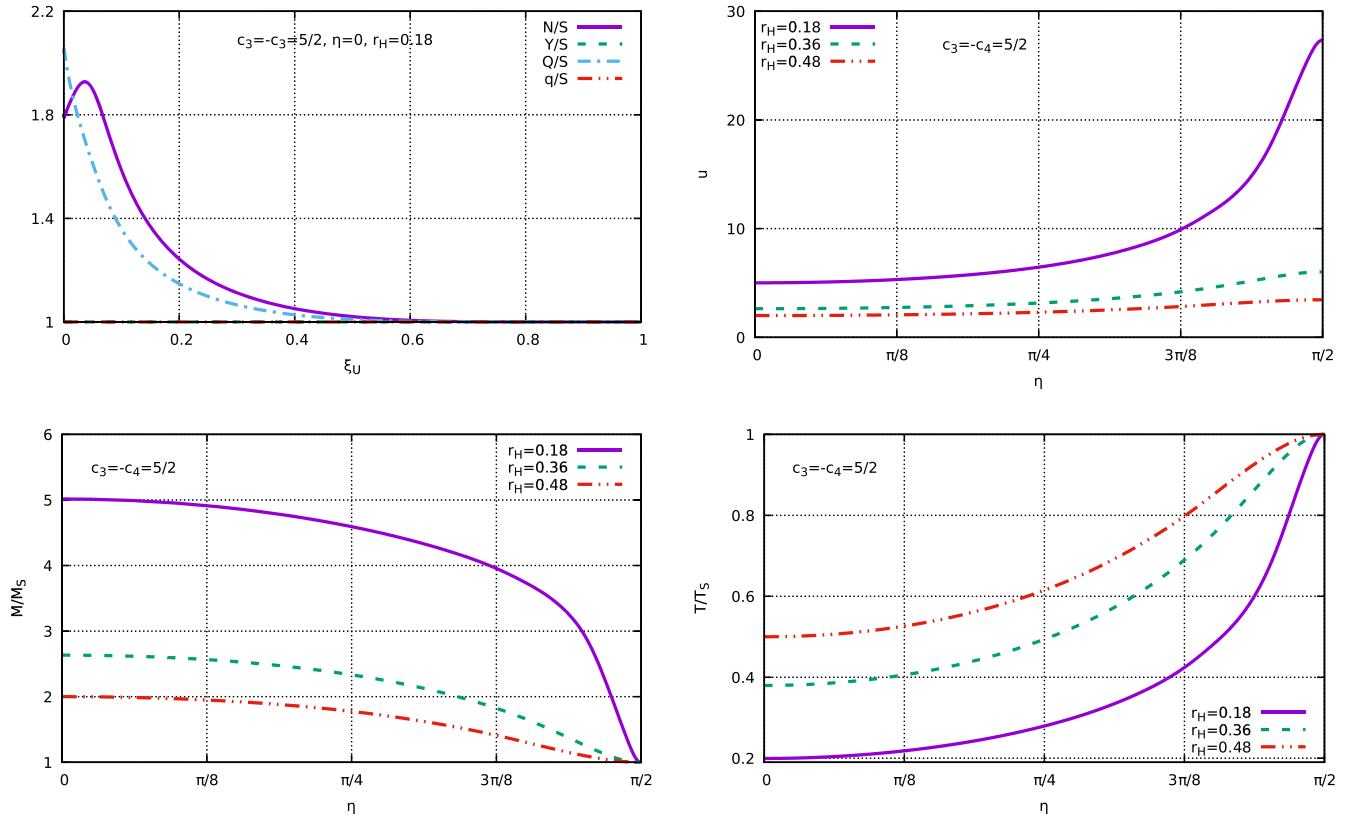

FIG. 4. Upper left: N/S, Y/S, Q/S, q/S with $S=\sqrt{1-U_H/U}$ against the compact variable $\xi_U=(U-U_H)/(U+U_H)$ for $\eta=0$. One has $Y/S=q/S=1$ hence the f metric is Schwarzschild. The other three panels show $u=U_H/r_H$, the ADM mass M, and the temperature T against η.

to each metric (the same is true for the temperature). If $\eta=\pi/2$ then the g metric is Schwarzschild hence $M=M_S$ and $T=T_S$. If $\eta=0$ then the f metric is Schwarzschild with a larger radius $U_H=ur_H$, hence the mass is larger, $M=U_H/2=uM_S$, while the temperature is smaller, $T=T_S/u$. Therefore, if $\eta=0$ then $M/M_S=u$ so that, for example, $u\approx 5$ for $r_H=0.18$, as seen in Fig. 4.

Figure 5 shows the dependence of u and M on c_3 in the case where $c_3=-c_4$. One can see that the solutions exist if only the value of $c_3=-c_4$ is not too small. Similarly, not all hairy black holes exist for however small values of r_H. As was noticed in [44], small r_H black holes exist if the coefficient b_3 in the potential (2.4) vanishes so that the cubic part of the potential is absent. In view of (2.15), this requires that $c_3=-c_4$, but this is not the only condition. Depending on the parameter values, one can distinguish the following two cases:

$$\text{I: } c_3\neq -c_4 \quad \text{or} \quad c_3=-c_4<1, \qquad \text{II: } c_3=-c_4\geq 1. \tag{9.2}$$

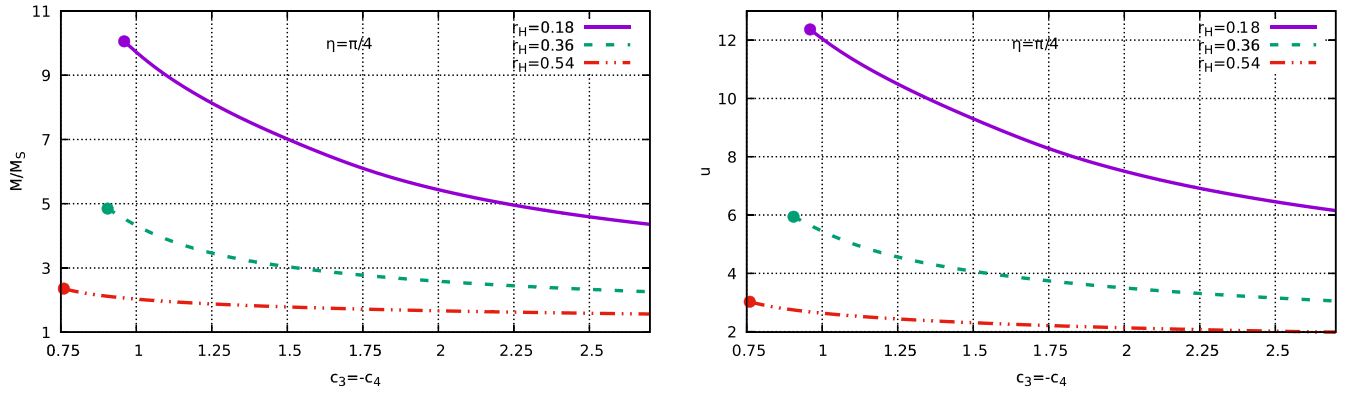

FIG. 5. The M/M_S (left) and $u=U_H/r_H$ (right) against $c_3=-c_4$.

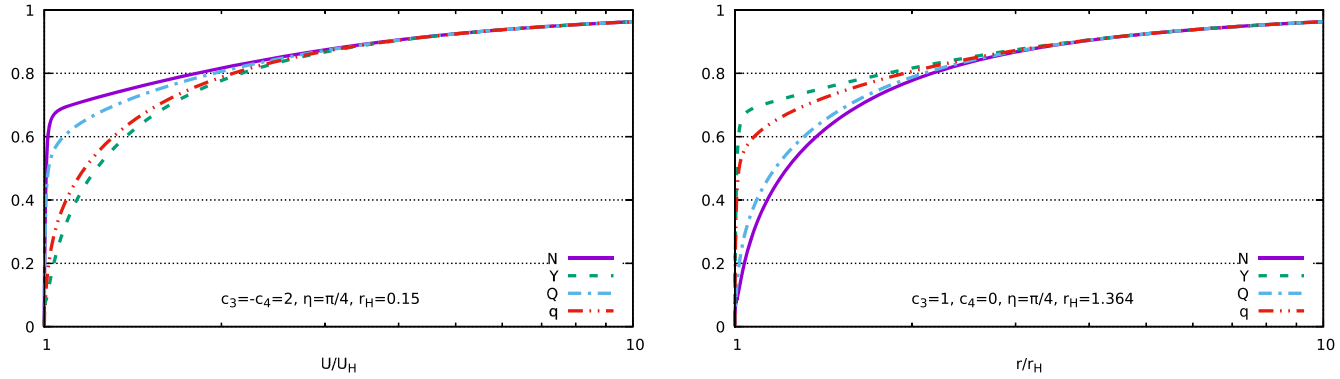

FIG. 6. The solution with $c_3 = -c_4 = 2$, $\eta = \pi/4$, $r_H = 0.15$ (left) and the dual solution with $c_3 = 1$, $c_4 = 0$, $\eta = \pi/4$, $r_H = 1.364$ (right). The curves on the two panels are exactly the same, up to the interchange $N \leftrightarrow Y$, $Q \leftrightarrow q$, $r/r_H \leftrightarrow U/U_H$.

In case I asymptotically flat hairy black holes exist only if $0 < r_H^{\min} \leq r_H < 0.86$ hence they cannot be arbitrarily small. In case II they exist for any $0 < r_H < 0.86$, although their f metric may be singular for small r_H. We shall see below in Sec. XI what happens when r_H approaches the lower bound.

A. Duality relation

The results described above in this section essentially reproduce those of Ref. [44], the only important difference being that we show solutions for different values of η, whereas Ref. [44] shows them only for $\eta = \pi/4$. However, starting from this moment and in the following two Sections we shall be describing new results.

Reference [44] finds solutions only below the GL point, for $r_H \leq 0.86$. At the same time, the consistency of the procedure requires that there should be asymptotically flat hairy black holes also for $r_H > 0.86$. This follows from the symmetry (4.16) of the equations, which now reads

$$\eta \to \frac{\pi}{2} - \eta, \qquad Q \leftrightarrow q, \qquad N \leftrightarrow Y, \qquad U \leftrightarrow r,$$
$$c_3 \to 3 - c_3, \qquad c_4 \to 4c_3 + c_4 - 6. \tag{9.3}$$

More precisely, this means that if for some values of η, c_3, c_4 there is a solution

$$Q(r), \quad q(r), \quad N(r), \quad Y(r), \quad U(r), \tag{9.4}$$

then for $\tilde\eta = \pi/2 - \eta$, $\tilde c_3 = 3 - c_3$, $\tilde c_4 = 4c_3 + c_4 - 6$ there should be the "dual" solution described by

$$\tilde Q(r) = q(w(r)), \quad \tilde q(r) = Q(w(r)), \quad \tilde N(r) = Y(w(r)),$$
$$\tilde Y(r) = N(w(r)), \qquad \tilde U(r) = w(r), \tag{9.5}$$

where $w(r)$ is the function inverse for $U(r)$, such that $U(w(r)) = r$. This duality correspondence relates between themselves black holes of different size, because (9.4) has the horizon at $r = r_H$ while the horizon of (9.5) is located where $w(r) = r_H$, that is at $r = \tilde r_H = U(r_H)$. One has

$$\tilde u = \frac{\tilde U(\tilde r_H)}{\tilde r_H} = \frac{r_H}{U(r_H)} = \frac{1}{u}. \tag{9.6}$$

Now, for hairy solutions with $r_H < 0.86$ one always has $U(r_H) > 0.86$ and $u = U(r_H)/r_H > 1$. It follows that their duals are characterized by $\tilde r_H > 0.86$ and by $\tilde u_H < 1$.

An explicit example of the duality relation is shown in Fig. 6, which presents on the left panel the solution for $c_3 = -c_4 = 2$, $\eta = \pi/4$, $r_H = 0.15$ for which $U(r_H) = 1.364$, hence $u = 1.364/0.15 = 2.42$. The duality implies that for $c_3 = 1$, $c_4 = 0$, $\eta = \pi/4$ there must be the dual solution with $r_H = 1.364$ and $u = 0.15/1.364 = 0.41$, which is indeed confirmed by our numerics. Plotting the first solution against U/U_H and the second one against r/r_H, as shown in Fig. 6, yields exactly the same curves, up to the interchange $N \leftrightarrow Y$, $Q \leftrightarrow q$.

It is unclear why solutions with $r_H > 0.86$ were not found in [44].

The duality is in fact a powerful tool for studying the solutions, because sometimes their properties may look puzzling in one description but become obvious within the dual description.

X. STABILITY ANALYSIS

In this section we analyze the stability of the hairy solutions by studying their perturbations within the ansatz described in Appendix B,

$$ds_g^2 = -Q^2dt^2 + \frac{dr^2}{N^2} + r^2d\Omega^2,$$
$$ds_f^2 = -(q^2 - \alpha^2Q^2N^2)dt^2 - 2\alpha\left(q + \frac{QNU'}{Y}\right)dtdr$$
$$+ \left(\frac{U'^2}{Y^2} - \alpha^2\right)dr^2 + U^2d\Omega^2, \tag{10.1}$$

where Q, q, N, Y, α, U are functions of r and t. The full set of the field equations in this case is shown in Appendix B. If we set $\alpha = 0$ and assume that nothing depends on time,

then we return back to the static case studied above. Therefore, small deviations from the static solutions are described by (10.1) with

$$\begin{aligned} Q(r,t) &= \overset{(0)}{Q}(r) + \delta Q(r,t), \\ q(r,t) &= \overset{(0)}{q}(r) + \delta q(r,t), \\ N(r,t) &= \overset{(0)}{N}(r) + \delta N(r,t), \\ Y(r,t) &= \overset{(0)}{Y}(r) + \delta Y(r,t), \\ U(r,t) &= \overset{(0)}{U}(r) + \delta U(r,t), \\ \alpha(r,t) &= \delta\alpha(r,t), \end{aligned} \tag{10.2}$$

where the functions $\overset{(0)}{Q}(r)$, $\overset{(0)}{q}(r)$, $\overset{(0)}{N}(r)$, $\overset{(0)}{Y}(r)$, $\overset{(0)}{U}(r)$ correspond to the background black hole solution while the perturbations $\delta Q, \delta q, \delta N, \delta Y, \delta U, \delta\alpha$ are small.

We therefore inject (10.2) to Eqs. (B5) and (B6) and linearize with respect to the perturbations. Linearizing the $G^0{}_1(g) = \kappa_1 T^0{}_1$ equation yields

$$\frac{2}{rNQ^2}\delta\dot{N} = \kappa_1 \frac{\mathcal{P}_1}{Q}\delta\alpha, \tag{10.3}$$

where $N, Q, \mathcal{P}_1$ relate to the static background, and we do not write their over sign "(0)" for simplicity. In the linear perturbation theory one can consistently separate the time variable by assuming the harmonic time dependence for all amplitudes (this would no longer be possible if nonlinear corrections are taken into account), so that we choose

$$\delta N(t,r) = e^{i\omega t}\delta N(r) \qquad \delta\alpha(t,r) = e^{i\omega t}\delta\alpha(r), \tag{10.4}$$

and similarly for $\delta Y, \delta Q, \delta q, \delta U$. Injecting to (10.3) yields the algebraic relation

$$\delta\alpha(r) = \frac{2i\omega}{rNQ\mathcal{P}_1}\delta N(r). \tag{10.5}$$

Linearizing similarly the $G^0{}_1(f) = \kappa_2 \mathcal{T}^0{}_1$ equation yields a linear relation between $\delta\alpha(r)$, $\delta Y(r)$, $\delta U(r)$. Using these two algebraic relations one finds that the three equations $G^0{}_0(g) = \kappa_1 T^0{}_0$, $G^0{}_0(f) = \kappa_2 \mathcal{T}^0{}_0$ and $\overset{(g)}{\nabla}_\mu T^\mu{}_0 = 0$ yield upon the linearization the same result. Therefore, among the 8 equations (B5), (B6) only 6 are independent (at least at the linearized level).

Taking all of this into account and linearizing similarly the remaining 3 equations $G^1{}_1(g) = \kappa_1 T^1{}_1$, $G^1{}_1(f) = \kappa_2 \mathcal{T}^1{}_1$ and $\overset{(g)}{\nabla}_\mu T^\mu{}_1 = 0$, one finds that all 6 perturbation amplitudes $\delta Q(r)$, $\delta q(r)$, $\delta N(r)$, $\delta Y(r)$, $\delta U(r)$ and $\delta\alpha(r)$ can be expressed in terms of a single master amplitude $\Psi(r)$ subject to the Schrödinger-type equation,

$$\frac{d^2\Psi}{dr_*^2} + (\omega^2 - V(r))\Psi = 0. \tag{10.6}$$

The master amplitude $\Psi(r)$ is a linear combination of $\delta N(r)$ and $\delta Y(r)$ with rather complicated coefficients whose explicit expression is not particularly illuminating, hence we do not show it explicitly. The potential $V(r)$ is also a complicated function of the background amplitudes that we do not show. The tortoise radial coordinate $r_* \in (-\infty, +\infty)$ is defined by the relation

$$dr_* = \frac{1}{a(r)}dr, \tag{10.7}$$

where the function $a(r)$ (also complicated) varies from 0 to 1 as r changes from r_H to ∞. The potential V always tends to zero at the horizon, for $r_* \to -\infty$, and it approaches unit value at infinity, for $r_* \to +\infty$. One should remember that our dimensionless variables are related to the dimensionful ones via $r = \mathrm{m}\mathrm{r}$, $r_H = \mathrm{m}\mathrm{r}_H$, $V = \mathrm{V}/\mathrm{m}^2$, $\omega = \boldsymbol{\omega}/\mathrm{m}$.

For the bald Schwarzschild background with $Q = q = N = Y = \sqrt{1 - r_H/r}$ and $U = r$, one has $a(r) = Q^2(r)$ and the potential reduces to

$$\begin{aligned} V(r) = &\left(1 - \frac{r_H}{r}\right) \\ &\times \left(1 + \frac{r_H}{r^3} + 6\frac{r_H(r_H - 2r) + r^3(r - 2r_H)}{(r_H + r^3)^2}\right), \end{aligned} \tag{10.8}$$

in agreement with Ref. [42]. In the flat space limit $r_H \to 0$ this reduces to $V(r) = 1 + 6/r^2$, which is the potential of a massive particle of unit mass (in units of the graviton mass) with spin $s = 2$.

Equation (10.6) defines the eigenvalue problem on the line $r_* \in (-\infty, +\infty)$. Solutions of this problem with $\omega^2 > 0$ describe scattering states of gravitons. In addition, there can be bound states with purely imaginary frequency $\omega = i\sigma$ and hence with $\omega^2 = -\sigma^2 < 0$. For such solutions the wave function Ψ is everywhere bounded and square-integrable, because one has $e^{+\sigma r_*} \leftarrow \Psi \to e^{-\sqrt{1+\sigma^2} r_*}$ as $-\infty \leftarrow r_* \to +\infty$, respectively. Such bound state solutions grow in time as $e^{i\omega t} = e^{\pm\sigma t}$. Therefore, they correspond to unstable modes of the background black holes.

A. Computing the eigenfrequencies

Our aim is to investigate a potential existence of negative modes with $\omega^2 < 0$ in the spectrum of the eigenvalue problem (10.6). If such modes exist, then the background black holes are unstable. If they do not exist, then the black holes are stable with respect to spherically symmetric

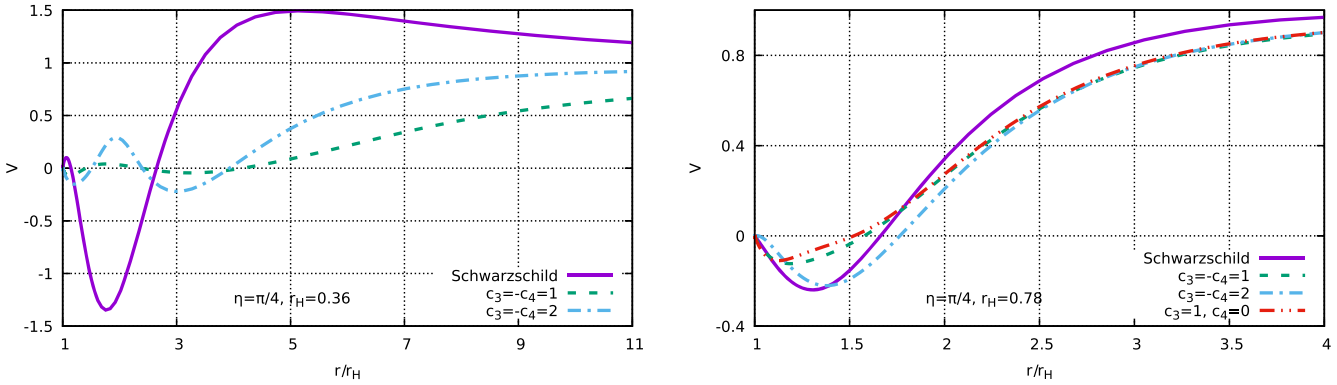

FIG. 7. Potential $V(r)$ for $r_H = 0.36$ (left) and for $r_H = 0.78$ (right) for different c_3, c_4 with $\eta = \pi/4$.

perturbations, which would strongly suggest that they should be stable with respect to all perturbations. Indeed, in most known cases the S-channel is usually the only place where the instability can reside (of course, this should be proven case to case).

The first thing to check is the shape of the potential $V(r)$, because if it is everywhere positive, then there are no bound states. We therefore show in Fig. 7 the potential $V(r)$ for the hairy backgrounds for several values of the event horizon size r_H and for different c_3, c_4, and we also show $V(r)$ for the bald Schwarzschild solution with the same r_H (it does not depend on c_3, c_4). We observe that in each case the potential vanishes at the horizon, then shows negative values in its vicinity, and then approaches unity as $r \to \infty$. Since the potential is not positive definite, bound states *may* exist, but their existence is not yet guaranteed.

We know that a bound state certainly exists for the bald Schwarzschild background with $r_H < 0.86$ [33,42]. When looking at the potentials for the hairy solution with $r_H = 0.78$ in Fig. 7, we notice that they are close to the Schwarzschild potential, hence a bound state could exist for these potentials as well.

In order to know whether bound states exist or not, we use the well-known Jacobi criterion [57] and construct the solution of the Schrödinger equation (10.6) with $\omega = 0$. If this solution $\Psi(r)$ crosses zero somewhere, then there are bound states. We start in the asymptotic region where the tortoise coordinate r_* becomes identical to the usual r, hence Eq. (10.6) reduces simply to $\Psi'' = \Psi$ so that the bounded solution is $\Psi = e^{-r}$. Then we extend this solution numerically toward small values of r, and we find that, depending on values of r_H, η, c_3, c_4, it may indeed show a zero as r approaches r_H. Therefore, there exists a bound state.

The next step is to actually find the bound state by solving the eigenvalue problem (10.6) with the potential $V(r)$ obtained by numerically solving the background equations. For this we set $\omega^2 = -\sigma^2$ and determine the local solutions at infinity and close to the horizon,

$$B(r - r_H)^{\sigma r_H} \leftarrow \Psi(r) \to e^{-\sqrt{1+\sigma^2}r} \quad \text{as } r_H \leftarrow r \to \infty, \tag{10.9}$$

where B is an integration constant. Then we apply the multiple shooting method and numerically extend the horizon solution toward large r, extending at the same time the large r solution toward small r. The two solutions meet at some intermediate point $r = r_0$, where the values of $\Psi(r_0)$ and $\Psi'(r_0)$ should agree. This gives two conditions to be fulfilled by adjusting the two parameters B and σ in (10.9), which finally yields the bound state solution on the whole line (see [58,59] for a review on the black hole perturbation theory and the tools that can be used to solve the perturbation equation).

The eigenfunctions Ψ against the ordinary radial coordinate r are shown in Fig. 8. They vanish at the horizon, then show a maximum, sometimes very close to the horizon, and then approach zero for $r \to \infty$.

As a result, we find the negative eigenvalues $\omega^2 < 0$ for all hairy black holes obtained in [44]. Therefore, all these solutions are unstable. It is worth emphasizing that all of them correspond to the particular choice $\eta = \pi/4$, hence $\kappa_1 = \kappa_2 = 1/2$. In order to test our method, we have also computed the negative mode for the bald Schwarzschild solution as in [42].

As seen in Fig. 9, the absolute value of the negative mode eigenvalue for the Schwarzschild solution is always larger than that for the hairy solutions. Therefore, the instability growth rate for the hairy black holes is not as large as for the Schwarzschild solution. In all cases, since one has $\omega = \boldsymbol{\omega}/\mathrm{m}$ where $\boldsymbol{\omega}$ is the dimensionful physical frequency, the instability growth time is $1/\boldsymbol{\omega} = 1/(\omega \mathrm{m})$. If we assume the graviton mass m to be very small and given by (5.5), then the instability growth time will be cosmologically large, hence the instability will not play any role. However, as we shall see below, it is preferable to assume that $1/\mathrm{m} \leq 10^6$ km according to (5.8), in which case the instability growth time will be less than 10^3 seconds, hence the instability is dangerous and should be avoided.

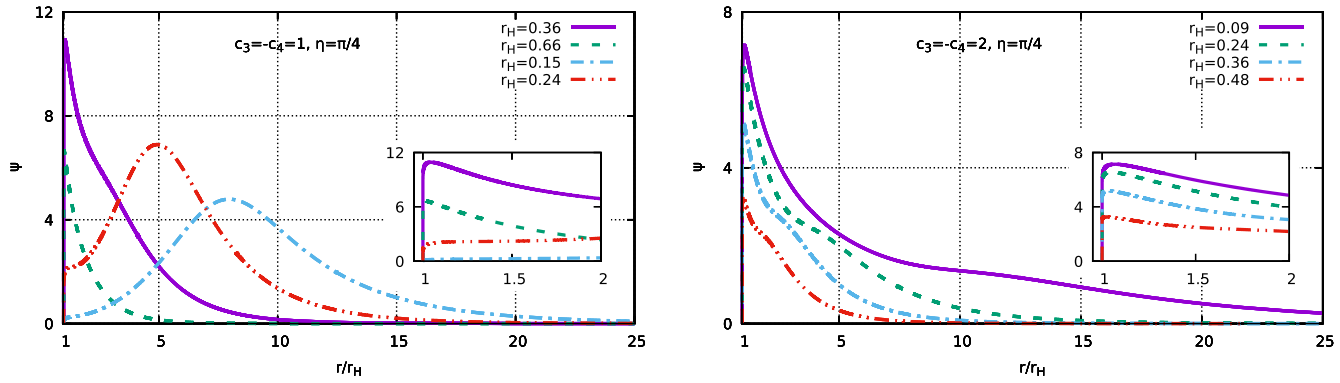

FIG. 8. Negative mode eigenfunctions $\Psi(r)$ for $\eta = \pi/4$ and different r_H, with $c_3 = -c_4 = 1$ (left) and $c_3 = -c_4 = 2$ (right). They vanish at the horizon and at infinity.

As seen in Fig. 9, the eigenvalue $\omega^2(r_H) < 0$ approaches zero when $r_H \to 0.86$, therefore all hairy black holes become then stable. However, they are no longer hairy in this limit, because they "lose their hair" and merge with the bald Schwarzschild solution. Near $r_H = 0.86$ all solutions are close to each other and ω^2 is close to zero for any c_3, c_4, η, while for smaller r_H the backgrounds and ω^2 become parameter dependent. The eigenvalue $\omega^2(r_H) < 0$ may approach zero also for type I solutions for a small $r_H \neq 0$ when they cease to exist. For example, for $c_3 = 1$, $c_4 = 0$, the hairy solution disappears at $r_H \sim 0.58$, and at the same time the eigenvalue ω^2 approaches zero, as seen in the insertion in Fig. 9.

The instability of hairy black holes is in fact a somewhat puzzling phenomenon, since it is unclear what they may decay into. Since the hairy solutions with $r_H < 0.86$ are more energetic than the bald Schwarzschild solution, they probably may approach the latter via absorbing and/or radiating away their hair during their decay. However, the bald Schwarzschild solution is also unstable for $r_H < 0.86$ and should decay into something.

The perturbative instability of the Schwarzschild solution in the massive bigravity theory is mathematically equivalent [33] to the Gregory-Laflamme instability of the vacuum black string in $D = 5$ [43]. It is known that the nonlinear development of the latter leads to the formation of an infinite string of "black hole beads" in $D = 5$, but the event horizon topology does not change [60]. This fact being established within the $D = 5$ vacuum GR, a similar scenario is not possible in the $D = 4$ bigravity theory, hence the fate of the bigravity black holes should be different. One possibility is that the black hole radiates away all of its energy within the S-channel (some radiative solutions are known explicitly [61,62]), but it is unclear what happens to the horizon, whether it disappears or not. In GR the horizon cannot disappear via a classical process [63], but in the bimetric theory the situation might be different.

Remarkably, we find that these puzzling issues are not omnipresent and the black holes can be stable if η is different from $\pi/4$. In Fig. 10 we show ω^2 against η for several values of r_H for solutions with $c_3 = -c_4 = 2$. One can see that $\omega^2(\eta) < 0$ approaches zero and the negative mode disappears in the hairy Schwarzschild limit when η approaches $\pi/2$. At the same time, the bald Schwarzschild solutions for the same r_H are certainly unstable. This is a

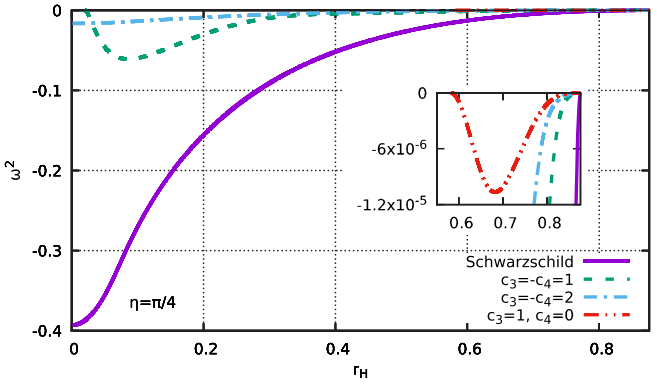

FIG. 9. The negative mode eigenvalue $\omega^2(r_H)$ for the hairy and for the bald Schwarzschild black holes against r_H for different values of c_3, c_4. In all cases $\eta = \pi/4$.

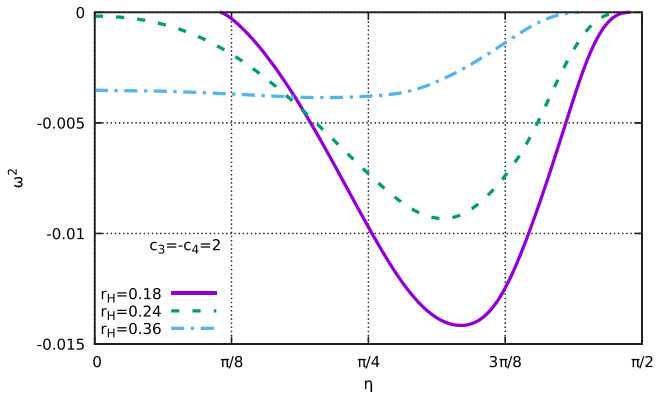

FIG. 10. The negative mode eigenvalue $\omega^2(\eta)$ for the hairy black holes with $c_3 = -c_4 = 2$.

very encouraging fact—we see that adding the hair to the black hole provides the stabilizing effect. As is seen in Fig. 10, the eigenvalue approaches zero also when η become small, if only r_H is also small, as seen in Fig. 10.

Summarizing the above discussion, for some parameter values the hairy black holes are unstable, but for other parameter values they can be stable. Below we shall describe a parameter choice leading to a large set of stable solutions.

XI. PARAMETER SPACE AND THE PHYSICAL SOLUTIONS

In this section we give a detailed description of particular subsets of solutions. Providing a complete classification of solutions depending on 4 parameters r_H, η, c_3, c_4 would be a very difficult task. We therefore adopt the following strategy: choosing the particular values

$$c_3 = -c_4 = 5/2 \tag{11.1}$$

which fulfill condition II in (9.2), we study the solutions for all possible r_H, η. Performing next the duality transformation gives us all possible solutions for

$$c_3 = 1/2, \qquad c_4 = 3/2, \tag{11.2}$$

which values fulfill condition I in (9.2). This approach reveals interesting and rather complex features which are presumably generic for any c_3, c_4.

Figure 11 shows the ADM mass $M(r_H)$ and the function $U_H(r_H)$ for several values of $\eta \in [0, \pi/2]$. As one can see, all curves $M(r_H)$ intersect at the GL point, $(r_H, M_H) = (0.86, 0.43)$, where all solutions bifurcate with the bald Schwarzschild solution,

$$N^2 = Q^2 = Y^2 = q^2 = 1 - \frac{0.86}{r}, \quad U = r, \tag{11.3}$$

whereas all curves $U_H(r_H)$ pass through the point $(r_H, U_H) = (0.86, 0.86)$. Away from the bifurcation point, the g metric still remains Schwarzschild if $\eta = \pi/2$, in which case $M(r_H)$ is a linear function,

$$\eta = \frac{\pi}{2}: \qquad N^2 = Q^2 = 1 - \frac{r_H}{r} \Rightarrow M = \frac{r_H}{2}, \tag{11.4}$$

but the f metric for these solutions is not Schwarzschild, even though both metrics have the same mass; as explained above, we call such solutions hairy Schwarzschild. For $\eta \neq \pi/2$ the mass depends nonlinearly on r_H.

Introducing the mass function $M(r)$ via $N^2(r) = 1–2M(r)/r$, Eq. (4.3) assumes the form

$$M'(r) = \kappa_1 \frac{r^2}{2}\left(\mathcal{P}_0 + U'\mathcal{P}_1 \frac{N}{Y}\right) \equiv \kappa_1 \rho, \tag{11.5}$$

from where the ADM mass

$$M = M(\infty) = \frac{r_H}{2} + \kappa_1 \int_{r_H}^{\infty} \rho dr \equiv M_{\text{bare}} + M_{\text{hair}}. \tag{11.6}$$

Here the "bare" mass $M_{\text{bare}} = r_H/2$ is determined only by the horizon radius and coincides with the mass of the Schwarzschild solution of radius r_H, whereas the mass M_{hair} expressed by the integral is the contribution of the massive hair distributed outside the horizon. As one can see in Fig. 11, one has $M > r_H/2$ if $r_H < 0.86$, hence the "hair mass" is positive and the hairy solutions are more energetic than the bare Schwarzschild black hole. However, the mass of the hair becomes negative above the GL point, where $r_H > 0.86$, and the hairy solutions are then less energetic

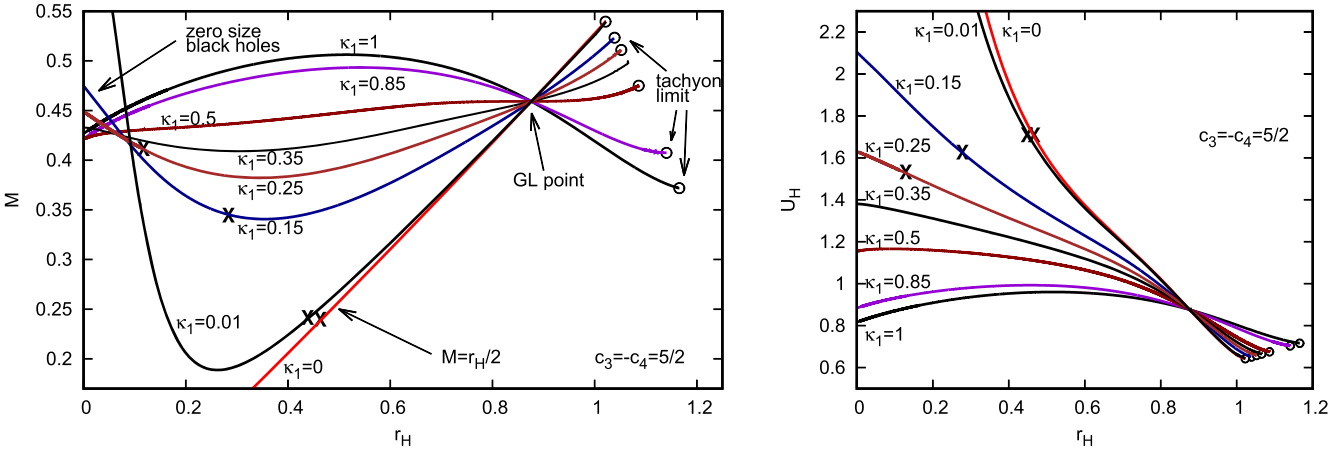

FIG. 11. The mass $M(r_H)$ (left) and the functions $U_H(r_H)$ (right) for the hairy solutions with $c_3 = -c_4 = 5/2$. The crosses mark the points on the left of which the f metric becomes singular. The hollow circles mark the termination points beyond which the solutions would become complex valued. When $\kappa_1 = \cos^2\eta \to 0$, the mass $M(r_H)$ develops a more and more profound minimum, while the values of $M(0)$ and $U_H(0)$ grow without bounds.

than the bare one. Therefore the energy density $\rho(r)$ can be negative. In fact, there are no reasons for which the standard energy conditions should be respected within the bigravity theory.

Each curve in Fig. 11 is defined only in a finite interval $r_H \in [0, r_H^{\max}(\eta)]$. It is very instructive to understand what happens at the boundaries of this interval.

A. The lower limit $r_H \to 0$

All the solutions extend down to arbitrarily small values of r_H. Remarkably, as seen in Fig. 11, except for $\eta = \pi/2$ the mass M does not vanish when $r_H \to 0$ but approaches a finite value, even though the bare mass $M_{\rm bare} = r_H/2 \to 0$. Therefore, all mass is contained in the hair mass in this limit, hence something remains even when the horizon size r_H shrinks to zero. A similar phenomenon is actually well known, since in many nonlinear field theories there are solutions describing a small black hole inside a soliton (for example, inside the magnetic monopole) [35]. Sending the horizon size to zero the black hole disappears, but its external nonlinear matter fields remain and become a gravitating soliton containing a regular origin in its center instead of the horizon. Therefore, the $r_H \to 0$ limit of a hairy black hole may correspond to a regular soliton.

One may expect the situation to be similar also in our case and that there is a limiting configuration to which the black hole solutions approach pointwise when $r_H \to 0$. Such a limiting configuration indeed exists; however, it seems to be singular and not of the regular soliton type. First, as seen in Fig. 11, the value of U_H which determines the size of the f horizon remains finite when $r_H \to 0$, hence the f geometry remains a black hole even in the limit. Secondly, as seen in Fig. 12, one has $N^2/S^2 \sim r$ for $r \leq 0.5$ for a solution with a very small r_H. However, one has $S = \sqrt{1 - r_H/r} \to 1$ as $r_H \to 0$, hence one has in this limit $N^2 \sim r$ and the limiting form of the g metric is something like a "zero size black hole." The numerical profiles shown in Fig. 12 suggest this limiting configuration to have the following structure at small r:

$$N^2 \sim Y^2 \sim Q^2 \sim q^2 \sim r, \qquad U = U_{\min} + \mathcal{O}(r). \tag{11.7}$$

The g geometry is singular since its Ricci invariant $R(g) = 2/r^2 + \mathcal{O}(1/r)$ at small r, but the f geometry remains of the regular black hole type because U does not vanish. Curiously, the temperature remains finite for $r_H \to 0$ and is always the same for both metrics. The limiting g temperature can be formally computed by assuming $N^2 = \alpha r$, $Q^2 = \beta r$ with $\alpha \approx 0.7$ and $\beta \approx 6$ from Fig. 12. Equation (6.5) then yields $T = \sqrt{\alpha\beta}/(4\pi) \approx 0.163$, which is very close to the value $T = 0.16$ for the solution with $r_H \sim 10^{-5}$ shown in Fig. 12. However, these considerations are of course purely formal since the zero size black hole cannot evaporate and further reduce its size, and the standard WKB arguments for the black hole evaporation do not apply because the geometry is singular at the horizon.

One should say that the f metric can become singular for small r_H because the q, Y amplitudes develop additional zeros outside the horizon. This happens along the parts of the curves on the left of the points marked by the crosses in Fig. 11. We have already discussed this phenomenon and said that we do not exclude such solutions from consideration because the f geometry is not observable and its singularities are invisible, while the g geometry that can be directly probed remains always regular. The physical parameters of the solutions such as the ADM mass also do not show anything special when the q, Y amplitudes starts to oscillate. The potential V in the perturbation equation (10.6) also remains regular. We therefore have no reason to exclude such solutions from consideration, and in fact they are necessary in order that the theory could describe black holes within a broad mass spectrum.

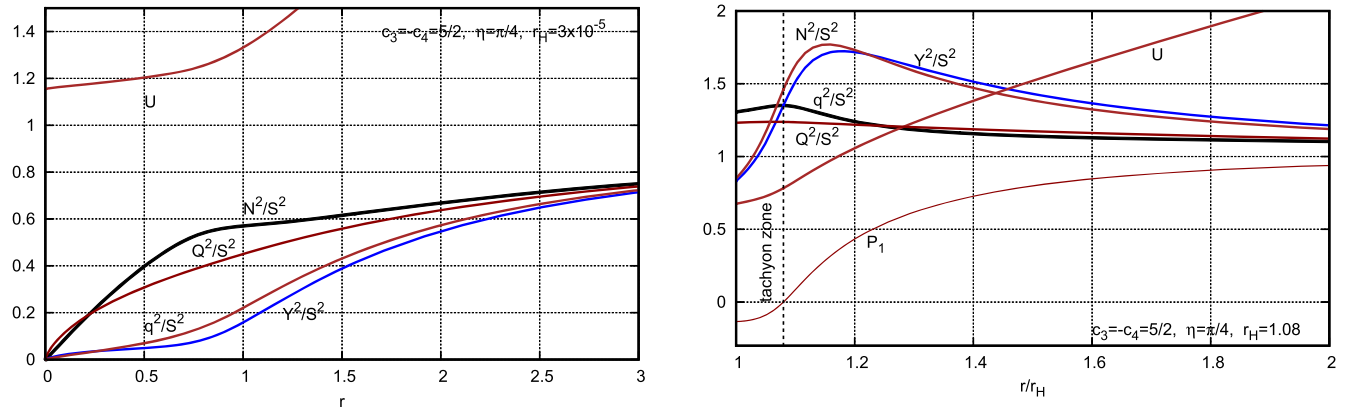

FIG. 12. Profiles of the solution with $r_H \sim 10^{-5}$ that is close to the zero size black hole (left), and of that close to the tachyon limit, with $D \sim 10^{-6}$ (right). One has $S^2 = 1 - r_H/r$. The amplitude $\mathcal{P}_1$ determines the graviton mass via (11.9) and the gravitons behave as tachyons if $\mathcal{P}_1 < 0$.

B. The upper "tachyon" limit $r_H \to r_H^{\max}(\eta)$

In this limit the solutions always remain regular and disappear after a fusion of roots of the algebraic equation (6.3) [or (A8)]. As explained above, this equation determines the horizon values of the solutions. Its two roots determine two solution branches, but only the root with $\sigma = +1$ gives rise to asymptotically flat solutions, the other branch showing a singularity of the g metric outside the horizon. When r_H increases, the determinant of (6.3) decreases and vanishes for some $r_H = r_H^{\rm tach}(\eta)$, then it becomes positive again, decreases again and vanishes for the second time for $r_H = r_H^{\max}(\eta) > r_H^{\rm tach}(\eta)$, after which it becomes negative and the procedure stops. Specifically, it turns out that the determinant of (6.3) factorizes,

$$\mathcal{D} \equiv \mathcal{B}^2 - 4\mathcal{A}\mathcal{C} = \mathcal{P}_1^2(r_H)D \Rightarrow \sqrt{\mathcal{D}} = \mathcal{P}_1(r_H)\sqrt{D}, \tag{11.8}$$

where $\mathcal{P}_1(r_H)$ is defined by (3.5) with $\mathbf{u} = U/r$ replaced by $u = U_H/r_H$ while D is a complicated function of r_H, U_H, η, c_3, c_4. When r_H increases, then $\mathcal{P}_1(r_H)$ crosses zero at some $r_H = r_H^{\rm tach}(\eta)$ while D remains positive, hence the square root $\sqrt{\mathcal{D}}$ changes sign. When r_H continues to increase, then D approaches zero and vanishes as $r_H \to r_H^{\max}(\eta)$. No further increase of r_H is possible since D would then be negative thus rendering the solutions complex valued.

Although the determinant $\mathcal{D}$ vanishes for $r_H = r_H^{\rm tach}(\eta)$ when $\mathcal{P}_1(r_H) = 0$ and also for $r_H = r_H^{\max}(\eta)$ when $D = 0$, the two solution branches never merge. Specifically, the two horizon values ν_H determined by (A8) merge when $\mathcal{D} = 0$, but a careful inspection reveals that y_H, U_H in (A5) and (A6) remain different for the two branches when $\mathcal{P}_1(r_H) = 0$. If $D = 0$ then all horizon values ν_H, y_H, U_H coincide for the two branches, but the derivatives y'_H defined by (A12) remain different. This is a consequence of the fact that the existence and uniqueness theorem applies only to regular points of the differential equations, whereas the event horizon $r = r_H$ is a singular point.

In the interval $r_H^{\rm tach}(\eta) < r_H < r_H^{\max}(\eta)$ the solutions show a "tachyon zone" near the horizon where the function $\mathcal{P}_1(r)$ defined by (3.5) is negative, as shown in the right panel in Fig. 12. Let us remember relation (2.13) for the Fierz-Pauli mass of gravitons obtained via linearizing the field equations around the flat background. This relation can be written as $\mathrm{m}_{\rm FP}^2 = \mathcal{P}_1(\infty)\ \mathrm{m}^2$. However, the equations can be similarly linearized around an arbitrary background solution, which yields in the spherically symmetric case the position-dependent mass term [64]

$$\mathrm{m}_{\rm FP}^2 = \mathcal{P}_1(r)\ \mathrm{m}^2. \tag{11.9}$$

Therefore, if $\mathcal{P}_1(r) < 0$ then the mass effectively becomes imaginary. As a result, solutions for $r_H > r_H^{\rm tach}$ show unphysical features, hence we call $r_H \to r_H^{\max}(\eta)$ the "tachyon limit." The horizon value y'_H diverges in this limit, but this seems to be an integrable divergence similar to $y'(r) \sim 1/\sqrt{r - r_H}$ and the limiting solution itself stays regular. We were able to approach this solution rather closely, as shown in Fig. 12 (right panel) which presents "an almost limiting" solution with the horizon value of the determinant $D \sim 10^{-6}$.

To recapitulate, hairy solutions exist only for $0 < r_H \leq r_H^{\max}(\eta)$.

C. The ADM mass

It is important that, unless $\kappa_1 = \cos^2\eta$ is very small, the ADM mass of all hairy solutions always varies within a finite range and can be neither very large nor very small, as seen in Fig. 11. It seems this fact was not recognized in Ref. [44], which always shows only the ratio M/r_H which diverges as $r_H \to 0$. However, the mass M remains finite for $r_H \to 0$. As seen in Fig. 11, the mass actually does not change much when r_H changes and always remains close to the GL value, which is the mass of the Schwarzschild solution with $r_H = 0.86$,

$$M \sim \frac{0.86}{2} = 0.43. \tag{11.10}$$

This means that the dimensionful mass (restoring for the moment the speed of light c and Newton's constant G)

$$\mathrm{M} = \frac{c^2 M}{G\,\mathrm{m}} \tag{11.11}$$

is always close to that of the Schwarzschild black hole of size $\mathrm{r}_H = 0.86/\mathrm{m}$, which is close to the Compton length of massive gravitons. As a result, one cannot assume the graviton mass m to be very small and of the order of the inverse Hubble radius as in (5.5). Indeed, this would imply the hairy black holes to be as heavy as the Schwarzschild black hole of a cosmological size—a physically meaningless result. However, assuming instead that $1/\mathrm{m} = \gamma \times 10^6$ km with $\gamma \in [0, 1]$ as in (5.8), which is consistent with the cosmological observations if κ_1 is parametrically small as expressed by (5.6), yields a physically acceptable result. The masses of the hairy black holes are then close to the mass of the Schwarzschild black hole of radius $\gamma \times 10^6$ km, that is $\mathrm{M} \sim 0.3 \times 10^6 \gamma \times \mathrm{M}_\odot$. If $\gamma \sim 1$ this gives the value typical for supermassive astrophysical black holes observed in the center of many galaxies.

If κ_1 is very small then the mass can deviate considerably from the GL value and can become very small or very large. As seen in Fig. 11, for small κ_1 the mass $M(r_H)$ shows a minimum: first it decreases with r_H, then reaches a minimal value $M_{\rm min}$, and then increases up to some $M(r_H = 0)$. For smaller values of κ_1 the minimum becomes more and more profound and the value $M_{\rm min}$ approaches zero while

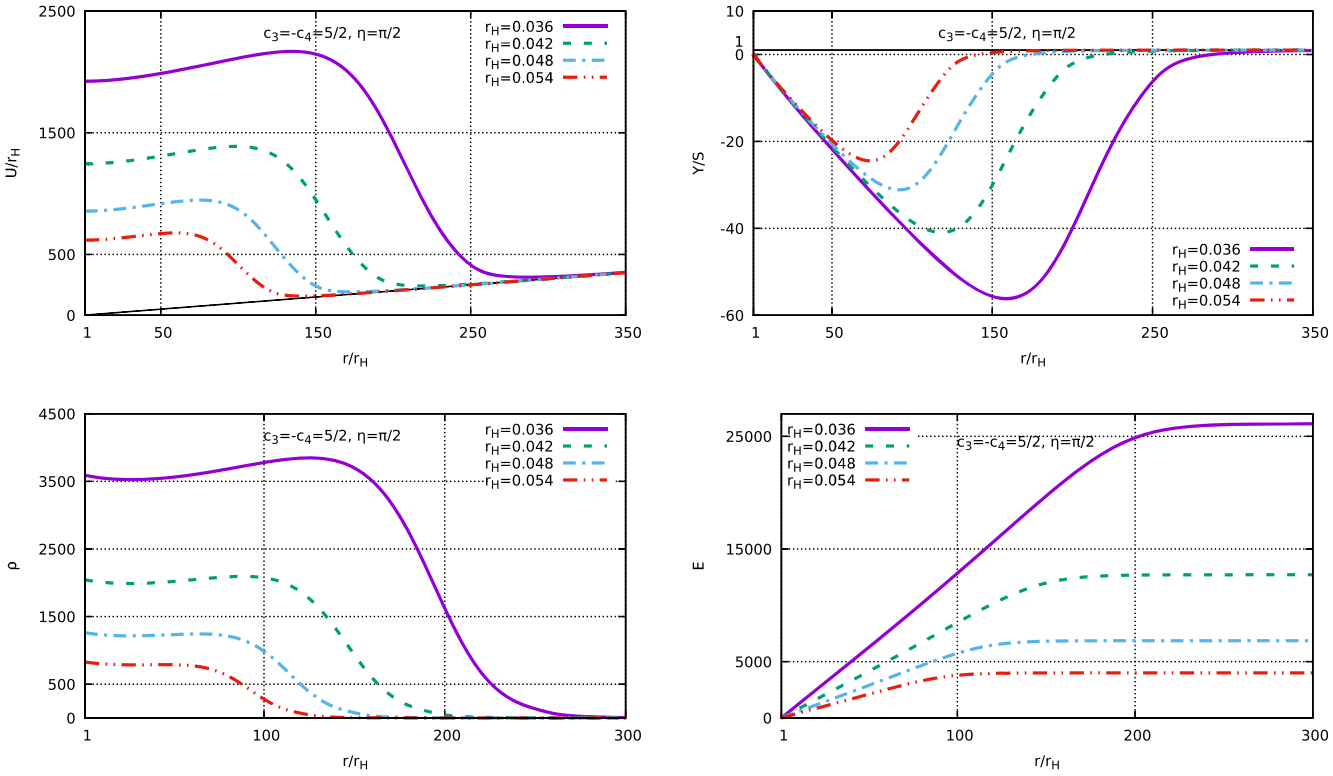

FIG. 13. The amplitudes $U(r)$, $Y(r)$, the "hair energy density" $\rho(r)$ and its integral $E(r)$ whose asymptotic value $E(\infty)$ is the "hair energy" for the hairy Schwarzschild solutions with $\kappa_1 = 0$ and $r_H \ll 1$.

$M(r_H = 0)$ becomes larger and larger. If κ_1 is extremely small as in (5.6), $\kappa_1 \leq 10^{-34}$, then the minimum value $M_{\min}$ is extremely close to zero. One has then $M(r_H) \approx r_H/2$ for $r > (r_H)_{\min}$ where $(r_H)_{\min}$ is very small, but in the region $r < (r_H)_{\min}$ the mass grows rapidly when $r_H \to 0$ up to a very large value $M(r_H = 0)$.

To get an approximation for $M(r_H)$ for very small κ_1, we consider the hairy Schwarzschild solutions with $\kappa_1 = 0$. Their g metric is Schwarzschild with all the hair contained in the f metric. It turns out that the Y, U amplitudes of the f metric depend very strongly on r_H if the latter is small. As seen in Fig. 13, in the horizon vicinity these amplitudes show very large values which apparently grow without bounds when $r_H \to 0$, although one always has $Y(r) \to 1$ and $U(r) \to r$ far away from the horizon. We inject these solutions to (11.5) and (11.6) to obtain the radial energy density $\rho(r)$ and $E(r) = \int_{r_H}^{r} \rho dr$. They also become very large when r_H decreases, as seen in Fig. 13. The asymptotic value $E(\infty)$ is the "hair energy." As seen in Fig. 13, the hair energy is large for small r_H, but it does not backreact and the g metric remains Schwarzschild if $\kappa_1 = 0$. However, the hair energy starts to backreact if $\kappa_1 \neq 0$. If $\kappa_1 \ll 1$ then one can deduce from Eq. (11.6) that

$$M = \frac{r_H}{2} + \kappa_1 E(\infty) + \mathcal{O}(\kappa_1^2), \tag{11.12}$$

where $E(\infty)$ is computed for $\kappa_1 = 0$. We evaluate numerically $E(\infty)$ for various values of r_H and obtain the following best fit approximation:

$$M \approx \frac{r_H}{2} + \kappa_1 \frac{a}{(r_H)^s}, \tag{11.13}$$

where $a = 0.0056$ and $s = 4.61$. Assuming that $\kappa_1 = \gamma^2 \times 10^{-34}$, this function shows an absolute minimum at

$$(r_H)_{\min} \approx 5.2\gamma^{0.35} \times 10^{-7}, \qquad M_{\min} \approx 3.1\gamma^{0.35} \times 10^{-7}, \tag{11.14}$$

whose dimensionful versions are obtained by multiplying by $1/\mathrm{m} = \gamma \times 10^6$ km (restoring again the speed of light and Newton's constant)

$$(\mathrm{r}_H)_{\min} = \frac{(r_H)_{\min}}{\mathrm{m}} \approx 0.52\gamma^{1.35} \text{ km},$$
$$\mathrm{M}_{\min} = \frac{c^2 M_{\min}}{G\,\mathrm{m}} \approx 0.2\gamma^{1.35} \times \mathrm{M}_\odot. \tag{11.15}$$

This determines the minimum mass for the hairy black holes. When r_H gets smaller still then the mass starts to grow, but it grows only up to a finite although very large

value as $r_H \to 0$ because the approximation (11.13) is not valid for however small r_H.

D. Parameter regions for solutions with $c_3 = -c_4 = 5/2$

Let us now collect all the facts together. The diagram in Fig. 14 shows the region in the (r_H, η) plane within which there are hairy black hole solutions. The low boundary of this region at $\eta = 0$ corresponds to solutions whose f metric is Schwarzschild, while the upper boundary at $\eta = \pi/2$ corresponds to solutions whose g metric is Schwarzschild. The left boundary corresponds to the limiting solutions with $r_H = 0$: the zero size black holes. The right boundary marks the tachyon limit beyond which the solutions would become complex-valued. The upper-left corner of the diagram contains solutions with a singular f geometry, but their g geometry, which is physically measurable, is regular.

The diagram also shows lines corresponding to the zero modes, $\omega^2 = 0$, of the perturbative eigenvalue problem (10.6). The vertical line corresponds to the GL value $r_H = 0.86$. The eigenvalue ω^2 changes sign when crossing these lines, therefore, the lines separate sectors where $\omega^2 > 0$ and hence the solutions are stable, from sectors where $\omega^2 < 0$ and the solutions are unstable. There are altogether two stable and two unstable sectors. It is worth noting that the stability region is now much larger than for solutions with $c_3 = -c_4 = 2$ considered in the previous section. One also notices that the tachyonic solutions are in the unstable sector.

Finally, the diagram shows the "physical region" corresponding to physically acceptable solutions. As explained above, for such solutions the coupling $\kappa_1 = \cos^2(\eta)$ should be very small for their mass not to be too large, hence η should be very close to $\pi/2$. The solutions should be stable, hence they should correspond to the sector where $\omega^2 > 0$.

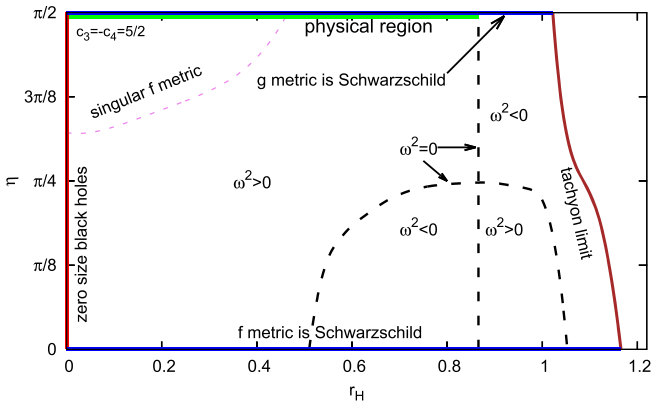

FIG. 14. The parameter region in the (r_H, η) plane corresponding to regular hairy black hole solutions with $c_3 = -c_4 = 5/2$. The dashed black $\omega^2 = 0$ lines separate stable and unstable sectors. The upper left corner contains solutions with a singular f metric; however, their g geometry is regular.

These conditions specify the physical region to be the thick (green online) line at the top of the diagram.

Physical solutions are therefore described by the g metric which is extremely close to Schwarzschild, since

$$G_{\mu\nu}(g) = \kappa_1 T_{\mu\nu}(g, f), \quad \text{where } \kappa_1 \leq 10^{-34}. \tag{11.16}$$

The "hairy features" of the solutions hidden in the f metric should be difficult to observe, unless in violent processes like black hole collisions producing large enough $T_{\mu\nu}(g, f)$ to overcome the 10^{-34} suppression. Summarizing, the static bigravity black holes should be extremely similar to the GR black holes, but their strong field dynamics is expected to be different.

As explained above, the physical region contains stable hairy black holes whose masses range from the minimal value $\sim 0.2\gamma^{1.35} \times \mathrm{M}_\odot$ up to the maximal value $\sim 0.3 \times 10^6 \gamma^{1.35} \times \mathrm{M}_\odot$ with $\gamma \in [0, 1]$. Yet heavier black holes also exist in the theory but they cannot be hairy and should be described by the "bald" Schwarzschild solution (1.2), which is stable for $r_H > 0.86$. Stable black holes with $\mathrm{M} \leq 0.2\gamma^{1.35} \times \mathrm{M}_\odot$ can only be of the type (1.1).

E. Parameter regions for dual solutions with $c_3 = 1/2$, $c_4 = 3/2$

Let us now see how the described above solutions look after the duality transformation (9.3). This transformation converts the parameter values (11.1) into (11.2), flips the sign of $\eta - \pi/4$ and swaps the Q, N, r with q, Y, U. Graphically, this amounts to relabelling the functions and plotting them against U instead of r. The ADM mass and temperature are invariant under duality. The stability property also does not change since, for example, if a solution is unstable and admits growing in time perturbations, then its dual version will contain the same growing modes and hence will be unstable as well.

Figure 15 shows the dual version of Fig. 11. The mass curves $M(r_H)$ still intersect in the GL point but they look quite different as compared to those in Fig. 11. In particular, not all of them are single valued. The reason is that the functions $U_H(r_H)$ in Fig. 11 are not always monotone, hence their inverses shown in Fig. 15 are not single valued. As a result, for each η such that $0 \leq \cos^2\eta \leq 0.6$ there are two different solutions with the same r_H but with different U_H, hence the curves $M(r_H)$ are not always single valued.

The solutions now exist for $r_H \in [r_H^{\min}(\eta), r_H^{\max}(\eta)]$. The lower limit $r_H^{\min}(\eta)$ corresponds to what used to be the upper limit before the duality—the tachyon solutions with vanishingly small horizon determinant D. The upper limit $r_H^{\max}(\eta)$ corresponds for small η to solutions whose g metric starts being singular. Before the duality these were solutions whose f metric started being singular while their g metric was regular. After the duality their g metric becomes singular, hence such solutions are no longer allowed and should be excluded. For larger values of η the right

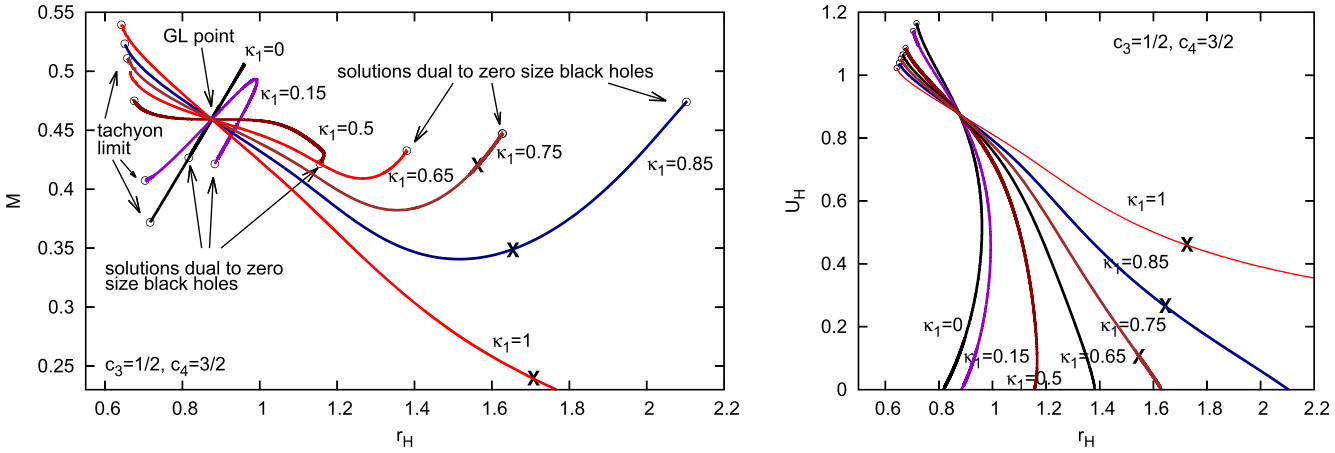

FIG. 15. The mass $M(r_H)$ (left) and the functions $U_H(r_H)$ (right) for the hairy black hole solutions with $c_3 = 1/2$, $c_4 = 3/2$. The crosses mark points on the right of which the g metric becomes singular, hence these pars of the curves correspond to unphysical solutions that should be excluded from consideration.

boundary $r_H^{\max}(\eta)$ corresponds to points where the two different solutions with the same r_H but with different U_H merge to each other.

The solutions below the GL point, for $r_H < 0.86$, are still more energetic than the solution with $\eta = \pi/2$, hence their hair mass $M_{\rm hair}$ is positive, whereas above the GL point it becomes negative. Finally, Fig. 16 shows the existence diagram in the (r_H, η) plane, together with the stability regions. The diagram now looks quite different as compared to that in Fig. 11, although it corresponds to essentially the same solutions, up to the duality transformation. Although the duality does not change stability, it interchanges positions of the stability sectors. Therefore, the physical region corresponding to stable solutions with η close to $\pi/2$ is now above the GL point, where the hair mass is negative. The physical solutions are again characterized by the g metric that is extremely close to Schwarzschild, but the novel feature is that now for each

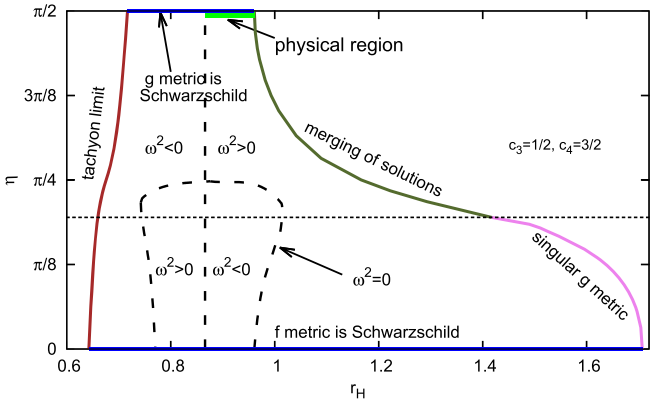

FIG. 16. The parameter region in the (r_H, η) plane corresponding to regular hairy black hole solutions with $c_3 = 1/2$, $c_4 = 3/2$. The dashed black $\omega^2 = 0$ lines separate stable and unstable sectors.

value of r_H from the physical region there are two different solutions whose g metrics are almost the same but the f metrics are different.

As one can see, the physical region in Fig. 15 is rather short and corresponds only to supermassive black holes with $0.86 < r_H < r_H^{\max}$. All black holes of smaller masses are unstable. Therefore, the parameter choice $c_3 = 1/2$, $c_4 = 3/2$ is not physically interesting.

XII. CONCLUDING REMARKS

To recapitulate, we presented above a detailed analysis of static and asymptotically flat black holes in the ghost-free massive bigravity theory. Extending the earlier result of [44], we find that for given values of the theory parameters c_3, c_4, η and for a given event horizon size varying within a finite range, $r_H \in [r_H^{\min}, r_H^{\max}]$, there are one or sometimes two different black holes supporting a nonlinear massive graviton hair, in addition to the "bald Schwarzschild" solution with $g_{\mu\nu} = f_{\mu\nu}$ described by (1.2). The hairy solutions are more energetic than the Schwarzschild one if $r_H < 0.86$ and they are less energetic otherwise. When r_H approaches the limiting values $r_H^{\min}$ or $r_H^{\max}$, the solutions either become complex valued or merge between themselves. For some values of c_3, c_4 zero-size black holes exist for which $r_H^{\min} = 0$ but the corresponding U_H remains finite. Depending on values of r_H, c_3, c_4, η, the hairy solutions can be either stable of unstable.

To avoid the hairy black holes being unphysically heavy, one is bound to assume the massive graviton Compton length to be $1/\mathrm{m} = \gamma \times 10^6$ km where the parameter γ may range in the interval [0, 1]. The agreement with the cosmological data is then achieved by assuming that $\kappa_1 = \cos^2\eta = \gamma^2 \times (\mathrm{M_{ew}}/\mathrm{M_{Pl}})^2 = \gamma^2 \times 10^{-34}$. The stable hairy black holes are described by a g metric which is extremely close to Schwarzschild, but their f metric is quite different. These black holes have the mass and size close to

those of ordinary black holes with the masses ranging from $\sim 0.2\gamma^{1.35} \times M_\odot$ to $\sim 0.3 \times 10^6 \gamma^{1.35} \times M_\odot$, the latter being the value typical for the supermassive astrophysical black holes if $\gamma \sim 1$. Yet heavier black holes in the theory should be bald. As a result, if the bigravity theory indeed applies to describe physics, the astrophysical black holes should support the hair hidden in the f metric.

Since the f metric is not coupled to matter and cannot be directly probed, while the deviation of the "visible" g metric from Schwarzschild is suppressed by the factor of $\kappa_1 = \gamma \times 10^{-34}$, the hairy black holes should normally be undistinguishable from the usual GR black holes. However, in violent processes like black hole coalescences the interaction between the two metrics may produce an energy momentum tensor strong enough to overcome the 10^{-34} suppression in $G_{\mu\nu}(g) = \kappa_1 T_{\mu\nu}(g, f)$. In this case the deviation from GR should become visible. Therefore, it is possible that signals from black hole mergers detected by LIGO/VIRGO [65] may carry information about the hairy structure of the black holes. One could expect a "hair imprint" in the signal to be stronger for *small* black holes, since we know that for small black holes the amplitudes U, Y of the f metric become very large, which should influence the $T_{\mu\nu}(g, f)$ of the merger. It is therefore possible that the hair imprints will be visible when smaller mass mergers (see [66] for a recent review) are detected. However, to actually determine the hair imprint in the signal would require calculations going beyond the scope of the present paper. We therefore leave this problem for a separate project and for the time being simply refer to the recent preprint [67] where calculations of this type are performed within the context of the ghost-gree massive gravity [8] [where the only static black holes are those described by (1.1)].

Finally, we should discuss the paper [45] that also considers black holes in the ghost-free massive bigravity theory. This paper presents essentially the same classification of different types of black holes as the one previously given in [18] but in a more refined way, extending it and paying attention to some subtle points. The paper addresses in particular the issue of convergence of the solutions to the flat background in the asymptotic region. Among other things, it claims that the Schwarzschild solution is the only asymptotically flat black hole in the theory. At the same time, the paper does not contain a rigorous proof of this statement but gives just a number of plausibility arguments, so that the claim should rather be viewed as a conjecture, as actually explicitly stated in some places of [45]. These arguments are as follows.

First of all, it was emphasized in [45] that the usual practice of starting the numerical integration not at the horizon $r = r_H$, which is a singular point of the differential equations, but at a regular nearby point $r = r_H + \epsilon$, as was done in [44], could in principle lead to numerical instabilities. We agree with this, and it is for this reason that we use the desingularization procedure (described in Appendix A below) which allows us to start the numerical integration exactly at $r = r_H$ (initial conditions exactly at $r = r_H$ were described also in [45]).

The paper [45] makes also another remark concerning the behavior at the horizon. It is known that in order to be able to *cross* the horizon, for example when studying geodesics, one cannot use the Schwarzschild coordinates and one should introduce instead regular at the horizon coordinates. These can be, for example, Eddington-Finkelshtein (EF) coordinates in which $g_{00} = g_{11} = 0$, $g_{01} = g_{10} \neq 0$. It was noticed in [45] that the f metric, when expressed in the same coordinates, generically does not have the same form, since it has $f_{11} \neq 0$, hence the two metrics cannot be simultaneously EF. We understand this, but this does not invalidate the background solutions (Ref. [45] agrees on this). The horizon geometries are regular, and if one wishes, one can use the same boundary conditions at the horizon to integrate inside the horizon to recover the interior solutions. Within the parametrization described in Appendix A, this is achieved by simply changing the sign of the numerical integration step.

Next, small initial deviations from the Schwarzschild solution via setting at the horizon $u = U_H/r_H = 1 + \epsilon$ were considered in [45]. Integrating the equations toward large r then yields metrics whose components diverge as $r \to \infty$ instead of approaching finite values. This observation, made already in [18], shows that there are no regular and asymptotically flat solutions *in a small vicinity* of the Schwarzschild solution. However, there can be regular solutions corresponding to u considerably deviating from unit value.

Finally, the paper [45] reproduces and analyzes (in Appendix A) one of the asymptotically flat solution (with a singular f metric) found in [44]. It obtains a pathological result, and the reason is the following. Appendix D of [45] describes the numerical method used—a straightforward integration starting from the horizon with the standard routine of *Mathematica*. This adequately produces the solution with a given precision, but only within a finite range of the radial coordinate r. If one integrates farther on trying to approach flat space, then the growing Ce^{+r} mode generically present in the solution leads to a rapid accumulation of numerical errors triggering a numerical instability. Trying to suppress this mode by adjusting the horizon boundary conditions, one typically observes the derivatives of some functions in the solution growing without bounds at a some finite r. Precisely this type of behavior at the end of the integration interval is seen in Fig. 11 in [45].

One cannot get asymptotically flat solutions within the numerical scheme adopted in [45], since pathological features arise in this way inevitably. This must be the reason behind the conviction that such solutions do not exist. However, all pathologies can be eliminated within the more elaborate numerical scheme described above—via suppressing the growing Ce^{+r} mode from the very beginning.

ACKNOWLEDGMENTS

We thank Francesco Torsello, Mikica Kocic, and Edvard Mörtsell for clarifying discussions and useful remarks. The work of M. S. V. was partly supported by the French National Center of Scientific Research within the collaborative French-Russian research program, Grant No. 289860, as well as by the Institute of Theoretical and Mathematical Physics at the Moscow University, and also by the Russian Government Program of Competitive Growth of the Kazan Federal University.

APPENDIX A: DESINGULARIZATION AT THE HORIZON

The horizon $r = r_H$ is a singular point of the differential equations—the derivatives N' and Y' expressed by Eqs. (4.23) are not defined at this point. The usual practice to handle this difficulty is to use the local power series expansions (6.1) and (6.2) to start the numerical integration not exactly at $r = r_H$ but at a nearby point with $r = r_H + \epsilon$ where ϵ is a small number. One may then hope that the results will not be very sensitive to the value of ϵ. However, in such an approach ϵ remains an arbitrary parameter not defined by any prescription. This inevitably affects the stability of the numerical procedure, which becomes evident when one studies the dependence of the solutions on the parameters.

At the same time, it is possible to reformulate the problem in such a way that the numerical integration starts exactly at $r = r_H$. Let us make the change of variables

$$N = S\nu, \qquad Y = Sy \quad \text{with} \quad S = \sqrt{1 - \frac{r_H}{r}}. \tag{A1}$$

The functions ν, y and their derivatives are defined also at $r = r_H$. Equations (4.3) and (4.4) then yield

$$\nu' = -\frac{\nu}{2r} + \frac{\mathcal{C}_1}{2\nu y r^2 S^2}, \quad y' = -\frac{yU'}{2U} + \frac{\mathcal{C}_2}{2\nu y r^2 U S^2}, \tag{A2}$$

where

$$\begin{aligned} \mathcal{C}_1 &= (r - r_H\nu^2 - \kappa_1 r^3 \mathcal{P}_0)y - \kappa_1 r^3 \mathcal{P}_1 U'\nu, \\ \mathcal{C}_2 &= \nu r^2(1 - \kappa_2 r^2 \mathcal{P}_2)U' - \kappa_2 r^4 \mathcal{P}_1 y - r_H U \nu y^2. \end{aligned} \tag{A3}$$

At the horizon the derivatives ν' and y' are finite, which requires that

$$\mathcal{C}_{1|_{r_H}} = 0, \qquad \mathcal{C}_{2|_{r_H}} = 0, \tag{A4}$$

from where one obtains the horizon values

$$U'_H = \left.\frac{(1 - \nu^2 - \kappa_1 r^2 \mathcal{P}_0)y}{\kappa_1 r^2 \mathcal{P}_1 \nu}\right|_{r_H}, \tag{A5}$$

$$y_H = \left.\frac{1 + (\kappa_2 r^2 \mathcal{P}_2 - 1)\nu^2 + \kappa_1\kappa_2(\mathcal{P}_0\mathcal{P}_2 - \mathcal{P}_1^2)r^4 - (\kappa_1 \mathcal{P}_0 + \kappa_2 \mathcal{P}_2)r^2}{\kappa_1 r \mathcal{P}_1 U \nu}\right|_{r_H}. \tag{A6}$$

At the same time, the horizon value of U' can be obtained from (4.23),

$$U'_H = \lim_{r \to r_H} \mathcal{D}_U(r, U, S\nu, Sy) \equiv \mathcal{D}_{UH}(r_H, U_H, \nu_H, y_H). \tag{A7}$$

This value must agree with the one given by (A5), which yields a condition on ν_H, and using (A6), this condition reduces [if b_k are chosen according to (2.15)] to a biquadratic equation

$$\mathcal{A}(\nu_H^2)^2 + \mathcal{B}\nu_H^2 + \mathcal{C} = 0, \tag{A8}$$

where the coefficients $\mathcal{A}$, $\mathcal{B}$, $\mathcal{C}$ are (rather complicated) functions of r_H, U_H. As a result, for given r_H, U_H there are two possible horizon values $\nu_H^{(1)}$ and $\nu_H^{(2)}$. Injecting to (A5) and (A6), this determines the horizon values y_H and U'_H. Finally, the horizon values of ν' and y' are obtained from (A2) by taking the $S \to 0$ limit and using l'Hopital's rule, which yields

$$\nu'_H = -\frac{\nu_H}{2r_H} + \frac{\mathcal{C}'_{1|_{r_H}}}{2r_H\nu_H y_H}, \quad y'_H = -\frac{y_H U'_H}{2U_H} + \frac{\mathcal{C}'_{2|_{r_H}}}{2r_H\nu_H y_H U_H}. \tag{A9}$$

There remains to compute the derivatives here. One has, for example,

$$\mathcal{C}'_{1|_{r_H}} = \left(\frac{\partial}{\partial r} + \nu'_H\frac{\partial}{\partial \nu} + y'_H\frac{\partial}{\partial y} + U'_H\frac{\partial}{\partial U} + U''_H\frac{\partial}{\partial U'}\right)\mathcal{C}_1(r, U, \nu, y, U')\Big|_{r=r_H, U=U_H, \nu=\nu_H, y=y_H} \tag{A10}$$

where the second derivative is similarly obtained from (A7),

$$U''_H = \left(\frac{\partial}{\partial r} + \nu'_H\frac{\partial}{\partial \nu} + y'_H\frac{\partial}{\partial y} + U'_H\frac{\partial}{\partial U}\right)\mathcal{D}_U(r, U, S\nu, Sy)\Big|_{r=r_H, U=U_H, \nu=\nu_H, y=y_H}, \tag{A11}$$

and similar expressions for $\mathcal{C}'_{2|_{r_H}}$. Injecting this to (A9) yields *linear* in ν'_H and y'_H relations, which can be resolved to give (we do not show explicit formulas in view of their complexity)

$$\nu'_H = \nu'_H(r_H, U_H, \nu_H, y_H), \qquad y'_H = y'_H(r_H, U_H, \nu_H, y_H). \tag{A12}$$

Summarizing the above discussion, the equations in the desingularized form read

$$\begin{aligned}
\nu' &= -\frac{\nu}{2r} + \frac{\mathcal{C}_1}{2\nu y r^2 S^2} \equiv \mathcal{F}_\nu(r, U, \nu, y),\\
y' &= -\frac{yU'}{2U} + \frac{\mathcal{C}_2}{2\nu y r^2 U S^2} \equiv \mathcal{F}_y(r, U, \nu, y),\\
U' &= \mathcal{D}_U(r, U, S\nu, Sy) \equiv \mathcal{F}_U(r, U, \nu, y),
\end{aligned} \tag{A13}$$

where $\mathcal{C}_1$ and $\mathcal{C}_2$ are defined by (A3) while $\mathcal{D}_U$ is the same as in (4.23). These equations apply for $r > r_H$, while at $r = r_H$ they should be replaced by

$$\begin{aligned}
\nu' &= \nu'_H(r_H, U_H, \nu_H, y_H),\\
y' &= y'_H(r_H, U_H, \nu_H, y_H),\\
U' &= U'_H(r_H, U_H, \nu_H, y_H),
\end{aligned} \tag{A14}$$

where ν'_H, y'_H, U'_H are defined by Eqs. (A5) and (A12). The horizon values r_H and $U_H \equiv u r_H$ can be arbitrary, while ν_H is not arbitrary but must fulfil the algebraic equation (A8), whereas y_H is determined by (A6). This formulation allows one to start the integration exactly at the horizon $r = r_H$ and then continue to the $r > r_H$ region.

APPENDIX B: FIELD EQUATIONS WITH TIME DEPENDENCE

Let us allow both metrics to depend on time, assuming that they are still spherically symmetric. The gauge freedom of reparametrizations of the t, r coordinates can be used to make the g metric diagonal, but the f metric will in general contain an off-diagonal term. The two metrics can be written as [10]

$$\begin{aligned}
ds_g^2 &= -Q^2 dt^2 + \frac{dr^2}{\Delta^2} + R^2 d\Omega^2,\\
ds_f^2 &= -(q^2 - \alpha^2 Q^2 \Delta^2) dt^2 - 2\alpha\left(q + \frac{Q\Delta}{W}\right) dt dr\\
&\quad + \left(\frac{1}{W^2} - \alpha^2\right) dr^2 + U^2 d\Omega^2,
\end{aligned} \tag{B1}$$

where $d\Omega^2 = d\theta^2 + \sin^2\theta d\phi^2$ and Q, q, Δ, W, α, U, R are functions of r and t.

One can check that the tensor

$$\gamma^\mu{}_\nu = \begin{pmatrix} q/Q & \alpha/Q & 0 & 0\\ -\alpha Q\Delta^2 & \Delta/W & 0 & 0\\ 0 & 0 & U/R & 0\\ 0 & 0 & 0 & U/R \end{pmatrix} \tag{B2}$$

has the property $\gamma^\mu{}_\sigma \gamma^\sigma{}_\nu = g^\mu{}_\sigma f^\sigma{}_\nu$. This tensor is used to compute the energy-momentum tensors $T^\mu{}_\nu$ and $\mathcal{T}^\mu{}_\nu$ in (2.7).

One can redefine the two amplitudes similarly to (4.1)

$$N = \Delta R', \qquad Y = WU', \tag{B3}$$

where the prime denotes the derivative with respect to r, and one can impose the gauge condition

$$R = r. \tag{B4}$$

As a result, the independent field equations (2.18) become

$$\begin{aligned}
&G^0_0(g) = \kappa_1 T^0{}_0, \qquad G^1_1(g) = \kappa_1 T^1{}_1, \qquad G^0_1(g) = \kappa_1 T^0{}_1,\\
&G^0_0(f) = \kappa_2 \mathcal{T}^0{}_0, \qquad G^1_1(f) = \kappa_2 \mathcal{T}^1{}_1, \qquad G^0_1(f) = \kappa_2 \mathcal{T}^0{}_1,
\end{aligned} \tag{B5}$$

plus two nontrivial components of the conservation condition $\overset{(g)}{\nabla}_\mu T^\mu{}_\nu = 0$,

$$\overset{(g)}{\nabla}_\mu T^\mu{}_0 = 0, \qquad \overset{(g)}{\nabla}_\mu T^\mu{}_1 = 0. \tag{B6}$$

Here one has explicitly

$$\begin{aligned}
&G(g)^0_0 = \frac{N^2 - 1}{r^2} + \frac{2NN'}{r}, \qquad G^1_1(g) = \frac{N^2 - 1}{r^2} + \frac{2N^2 Q'}{rQ},\\
&G^0_1(g) = \frac{2\dot{N}}{rNQ^2},
\end{aligned} \tag{B7}$$

where the dot denotes the partial derivative with respect to t, while

$$\begin{aligned}
&T^0{}_0 = -\mathcal{P}_0 - \mathcal{P}_1 \frac{NU'}{Y}, \qquad T^1{}_1 = -\mathcal{P}_0 - \mathcal{P}_1 \frac{q}{Q},\\
&T^0{}_1 = \mathcal{P}_1 \frac{\alpha}{Q},
\end{aligned} \tag{B8}$$

where $\mathcal{P}_m$ are defined in (3.5). The components of the second stress-energy tensor are

$$\begin{aligned}
\mathcal{T}^0{}_0 &= -\frac{r^2}{NU^2\mathcal{A}}(\mathcal{P}_1 qY + \mathcal{P}_2(\alpha^2 N^2 QY + qNU')),\\
\mathcal{T}^1{}_1 &= -\frac{r^2}{U^2\mathcal{A}}(\mathcal{P}_1 QU' + \mathcal{P}_2(\alpha^2 NQY + qU')),\\
\mathcal{T}^0{}_1 &= -\frac{r^2}{NU^2\mathcal{A}}\mathcal{P}_1 Y\alpha,
\end{aligned} \tag{B9}$$

where $\mathcal{A} = NQY\alpha^2 + qU'$. The components of the Einstein tensor for $f_{\mu\nu}$, are complicated:

$$
\begin{aligned}
G(f)^0{}_0 = &-\frac{1}{U^2 Y \mathcal{A}^3}(N^3Q^3Y^4\alpha^6 + (-NQ\dot{U}^2Y^4 + N^3Q^3U'^2Y^4 + 2N^3Q^3UU''Y^4 \\
&+ 3N^2qQ^2U'Y^3)\alpha^4 + (-2NQU\dot{U}\,\dot{\alpha}\,Y^4 - 2qQU\dot{U}N'Y^4 + 2NQU\dot{U}q'Y^4 \\
&- 2NqU\dot{U}Q'Y^4 + 2NqQ\dot{U}U'Y^4 - 2N^3Q^3UU'\alpha'Y^4 + 2NqQU\dot{U}'Y^4 \\
&+ 2N^2Q^2\dot{U}U'^2Y^3 + 2N^2Q^2UU'\dot{U}'Y^3 + 2N^2Q^2U\dot{U}U''Y^3 - 2N^2Q^2U\dot{U}U'Y'Y^2)\alpha^3 \\
&+ (-Nq^2QU'^2Y^4 + 2q^2QUN'U'Y^4 - 2NqQUq'U'Y^4 + 2Nq^2UQ'U'Y^4 \\
&- 2NqQU\dot{U}\alpha'Y^4 - 2Nq^2QUU''Y^4 + N^2qQ^2U'^3Y^3 + 2NqQ^2UN'U'^2Y^3 \\
&- 2N^2Q^2Uq'U'^2Y^3 + 2N^2qQUQ'U'^2Y^3 - q\dot{U}^2U'Y^3 - 2N^2Q^2U\dot{U}U'\alpha'Y^3 \\
&+ NQ\dot{U}^2U'^2Y^2 + 3Nq^2QU'^2Y^2 + 2N^2qQ^2UU'^2Y'Y^2 + 2NQU\dot{U}U'\dot{U}'Y^2 \\
&- 2NQU\dot{U}\,\dot{Y}\,U'^2Y)\alpha^2 + (4Nq^2QUU'\alpha'Y^4 + 2q^2\dot{U}U'^2Y^3 - 2qU\dot{U}\,\dot{\alpha}\,U'Y^3 \\
&+ 2N^2qQ^2UU'^2\alpha'Y^3 + 2q^2UU'\dot{U}'Y^3 - 2q^2U\dot{U}U''Y^3 + 2NqQ\dot{U}U'^3Y^2 \\
&+ 2qQU\dot{U}N'U'^2Y^2 - 2NQU\dot{U}q'U'^2Y^2 + 2NqU\dot{U}Q'U'^2Y^2 + 2q^2U\dot{U}U'Y'Y^2 \\
&+ 2NqQUU'^2\dot{U}'Y^2)\alpha - q^3Y^3U'^3 + qY\dot{U}^2U'^3 + q^3YU'^3 - 2qU\dot{U}\,\dot{Y}\,U'^3 \\
&- 2q^3UY^2U'^2Y' + 2NqQUY^2\dot{U}U'^2\alpha' + 2q^2UY^3\dot{U}U'\alpha' + 2qUY\dot{U}U'^2\dot{U}'), \\
G(f)^0{}_1 = &-\frac{2}{UY\mathcal{A}^3}((-Q\dot{U}N'Y^4 - N\dot{U}Q'Y^4 + NQ\dot{U}'Y^4)\alpha^4 + (-NQ\dot{\alpha}U'Y^4 \\
&+ qQN'U'Y^4 + NqQ'U'Y^4 - NQ\dot{U}\alpha'Y^4 - NqQU''Y^4 + NQ^2N'U'^2Y^3 \\
&+ N^2QQ'U'^2Y^3 - N^2Q^2U'U''Y^3)\alpha^3 + (2NqQU'\alpha'Y^4 - \dot{U}q'U'Y^3 + qU'\dot{U}'Y^3 \\
&+ 2N^2Q^2U'^2\alpha'Y^3 - q\dot{U}U''Y^3 + Q\dot{U}N'U'^2Y^2 + N\dot{U}Q'U'^2Y^2 + q\dot{U}U'Y'Y^2 \\
&- NQ\dot{U}U'U''Y^2 - NQ\dot{Y}U'^3Y + NQ\dot{U}U'^2Y'Y)\alpha^2 + (-q\dot{\alpha}U'^2Y^3 + qq'U'^2Y^3 \\
&+ q\dot{U}U'\alpha'Y^3 + NQq'U'^3Y^2 - q^2U'^2Y'Y^2 + 2NQ\dot{U}U'^2\alpha'Y^2 - NqQU'^3Y'Y)\alpha - q\dot{Y}U'^4 + Y\dot{U}q'U'^3), \\
G(f)^1{}_1 = &-\frac{1}{U^2\mathcal{A}^3}(N^3Q^3Y^3\alpha^6 + (-NQ\dot{U}^2Y^3 + N^3Q^3U'^2Y^3 + 2QU\dot{N}\,\dot{U}\,Y^3 + 2NU\dot{Q}\,\dot{U}\,Y^3 \\
&- 2NQU\ddot{U}Y^3 + 2N^2Q^3UN'U'Y^3 + 2N^3Q^2UQ'U'Y^3 + 3N^2qQ^2U'Y^2)\alpha^4 \\
&+ (2NQU\dot{U}\,\dot{\alpha}\,Y^3 - 2qQU\dot{N}U'Y^3 + 2NQU\dot{q}U'Y^3 - 2NqU\dot{Q}U'Y^3 \\
&+ 2NqQ\dot{U}U'Y^3 + 2N^3Q^3UU'\alpha'Y^3 + 2NqQU\dot{U}'Y^3 + 2N^2Q^2\dot{U}U'^2Y^2 \\
&+ 4N^2Q^2UU'\dot{U}'Y^2 - 2N^2Q^2U\dot{Y}U'^2Y)\alpha^3 + (-Nq^2QU'^2Y^3 - 2NqQU\dot{\alpha}U'Y^3 \\
&- 2NqQUq'U'Y^3 + N^2qQ^2U'^3Y^2 - 2N^2Q^2U\dot{\alpha}U'^2Y^2 + 2NqQ^2UN'U'^2Y^2 \\
&+ 2N^2qQUQ'U'^2Y^2 - q\dot{U}^2U'Y^2 + 2U\dot{q}\,\dot{U}\,U'Y^2 - 2qU\ddot{U}U'Y^2 + 2qU\dot{U}\dot{U}'Y^2 \\
&+ NQ\dot{U}^2U'^2Y + 3Nq^2QU'^2Y - 2QU\dot{N}\,\dot{U}\,U'^2Y - 2NU\dot{Q}\,\dot{U}\,U'^2Y + 2NQU\ddot{U}U'^2Y \\
&- 2qU\dot{U}\,\dot{Y}\,U'Y + 2NQU\dot{U}U'\dot{U}'Y - 2NQU\dot{U}\,\dot{Y}\,U'^2)\alpha^2 + (2qQUY\dot{N}U'^3 \\
&- 2NQUY\dot{q}U'^3 + 2NqUY\dot{Q}U'^3 + 2NqQY\dot{U}U'^3 + 2q^2Y^2\dot{U}U'^2 + 2q^2UY\dot{Y}U'^2 \\
&- 4NQUY\dot{U}\,\dot{\alpha}\,U'^2 + 2N^2qQ^2UY^2\alpha'U'^2 + 2NqQUY\dot{U}'U'^2 - 2qUY^2\dot{U}\,\dot{\alpha}\,U')\alpha \\
&+ q^3U'^3 - q^3Y^2U'^3 + q\dot{U}^2U'^3 - 2U\dot{q}\,\dot{U}\,U'^3 + 2NqQUY\dot{\alpha}U'^3 + 2qU\ddot{U}U'^3 \\
&+ 2q^2UY^2\dot{\alpha}U'^2 - 2q^2UY^2q'U'^2).
\end{aligned}
\tag{B10}
$$

Finally, there are two nontrivial components of the conservation law,

$$\overset{(g)}{\nabla}_\mu T^\mu{}_0 = -\mathcal{P}_1\left(\alpha N' N Q + 2\alpha N^2 Q + \alpha' N^2 Q + \frac{q\dot{N}}{NQ} + \frac{N\dot{U}'}{Y} - \frac{NU'\dot{Y}}{Y^2}\right) - \frac{d\mathcal{P}_0}{r}(\alpha N^2 Q + \dot{U}) - \frac{d\mathcal{P}_1}{r}\left(\alpha N^2 Q U' + \frac{N\dot{U}U'}{Y}\right),$$
$$\overset{(g)}{\nabla}_\mu T^\mu{}_1 = \mathcal{P}_1\left(\frac{\dot{\alpha}}{Q} - \frac{\alpha\dot{N}}{NQ} - \frac{q'}{Q} + \frac{NQ'U'}{QY}\right) + \frac{d\mathcal{P}_1}{r}\left(\alpha^2 N^2 + \frac{\alpha\dot{U}}{Q} + \frac{qNU'}{QY} - \frac{qU'}{Q}\right) + \frac{d\mathcal{P}_0}{r}\left(\frac{NU'}{Y} - U'\right), \tag{B11}$$

where $d\mathcal{P}_m$ are defined in (4.10). Equations (B5), (B6) comprise a system of 8 equations for 6 functions Q, q, Δ, W, α, U. For this system not to be overdetermined, only 6 equations out of 8 should be independent. As shown in Sec. X, this indeed happens at least for small α, when the perturbative analysis of the equations shows that some of them coincide.

[1] A. Riess *et al.*, Astron. J. **116**, 1009 (1998).
[2] S. Perlmutter *et al.*, Astrophys. J. **517**, 565 (1999).
[3] M. Fierz and W. Pauli, Proc. R. Soc. A **173**, 211 (1939).
[4] H. van Dam and M. J. G. Veltman, Nucl. Phys. **B22**, 397 (1970).
[5] V. I. Zakharov, JETP Lett. **12**, 312 (1970), https://ui.adsabs.harvard.edu/abs/1970JETPL..12..312Z/abstract.
[6] A. I. Vainshtein, Phys. Lett. **39B**, 393 (1972).
[7] D. G. Boulware and S. Deser, Phys. Rev. D **6**, 3368 (1972).
[8] C. de Rham, G. Gabadadze, and A. J. Tolley, Phys. Rev. Lett. **106**, 231101 (2011).
[9] S. F. Hassan and R. A. Rosen, J. High Energy Phys. 02 (2012) 126.
[10] M. Volkov, J. High Energy Phys. 01 (2012) 035.
[11] M. von Strauss, A. Schmidt-May, J. Enander, E. Mortsell, and F. Hassan, J. Cosmol. Astropart. Phys. 03 (2012) 042.
[12] D. Comelli, M. Crisostomi, F. Nesti, and L. Pilo, J. High Energy Phys. 03 (2012) 067.
[13] Y. Akrami, S. Hassan, F. Könnig, A. Schmidt-May, and A. R. Solomon, Phys. Lett. B **748**, 37 (2015).
[14] E. Mortsell and J. Enander, J. Cosmol. Astropart. Phys. 10 (2015) 044.
[15] K. Aoki, K.-I. Maeda, and R. Namba, Phys. Rev. D **92**, 044054 (2015).
[16] M. Lüben, E. Mörtsell, and A. Schmidt-May, Classical Quantum Gravity **37**, 047001 (2020).
[17] M. Högås, F. Torsello, and E. Mörtsell, J. Cosmol. Astropart. Phys. 04 (2020) 046.
[18] M. S. Volkov, Phys. Rev. D **85**, 124043 (2012).
[19] S. V. Sushkov and M. S. Volkov, J. Cosmol. Astropart. Phys. 06 (2015) 017.
[20] M. Volkov, Classical Quantum Gravity **30**, 184009 (2013).
[21] C. J. Isham and D. Storey, Phys. Rev. D **18**, 1047 (1978).
[22] M. Gurses, Phys. Rev. D **20**, 1019 (1979).
[23] M. Gurses, J. Phys. A **14**, 1957 (1981).
[24] C. Isham, A. Salam, and J. Strathdee, Phys. Rev. D **3**, 867 (1971).
[25] E. Babichev and A. Fabbri, Phys. Rev. D **89**, 081502 (2014).
[26] M. S. Volkov, Lect. Notes Phys. **892**, 161 (2015).
[27] Z. Berezhiani, D. Comelli, F. Nesti, and L. Pilo, J. High Energy Phys. 07 (2008) 130.
[28] D. Comelli, M. Crisostomi, F. Nesti, and L. Pilo, Phys. Rev. D **85**, 024044 (2012).
[29] E. Babichev and A. Fabbri, J. High Energy Phys. 07 (2014) 016.
[30] E. Babichev and A. Fabbri, Phys. Rev. D **90**, 084019 (2014).
[31] R. A. Rosen, Phys. Rev. D **98**, 104008 (2018).
[32] E. Babichev, R. Brito, and P. Pani, Phys. Rev. D **93**, 044041 (2016).
[33] E. Babichev and A. Fabbri, Classical Quantum Gravity **30**, 152001 (2013).
[34] M. C. Volkov and D. V. Gal'tsov, Pis'ma Zh. Eksp. Teor. Fiz. **50**, 312 (1989) [JETP Lett. **50**, 346 (1989)], https://ui.adsabs.harvard.edu/abs/1989PZETF..50..312V/abstract.
[35] M. S. Volkov and D. V. Gal'tsov, Phys. Rep. **319**, 1 (1999).
[36] M. S. Volkov, arXiv:1601.08230.
[37] C. Deffayet and T. Jacobson, Classical Quantum Gravity **29**, 065009 (2012).
[38] M. Banados, A. Gomberoff, and M. Pino, Phys. Rev. D **84**, 104028 (2011).
[39] W. Press, S. Teukolsky, W. Vetterling, and B. Flannery, *Numerical Recipes 3rd Edition: The Art of Scientific Computing* (Cambridge University Press, New York, 2007).
[40] J. Enander and E. Mortsell, J. Cosmol. Astropart. Phys. 11 (2015) 023.
[41] K. Aoki, K.-I. Maeda, and M. Tanabe, Phys. Rev. D **93**, 064054 (2016).
[42] R. Brito, V. Cardoso, and P. Pani, Phys. Rev. D **88**, 023514 (2013).
[43] R. Gregory and R. Laflamme, Phys. Rev. Lett. **70**, 2837 (1993).
[44] R. Brito, V. Cardoso, and P. Pani, Phys. Rev. D **88**, 064006 (2013).

[45] F. Torsello, M. Kocic, and E. Mortsell, Phys. Rev. D **96**, 064003 (2017).
[46] P. Breitenlohner, P. Forgacs, and D. Maison, Nucl. Phys. **B383**, 357 (1992).
[47] P. Breitenlohner, P. Forgacs, and D. Maison, Nucl. Phys. **B442**, 126 (1995).
[48] P. Breitenlohner, P. Forgacs, and D. Maison, Commun. Math. Phys. **163**, 141 (1994).
[49] S. Hassan and R. A. Rosen, J. High Energy Phys. 04 (2012) 123.
[50] S. Alexandrov, Gen. Relativ. Gravit. **46**, 1639 (2014).
[51] V. O. Soloviev, arXiv:2006.16230.
[52] S. Hassan, A. Schmidt-May, and M. von Strauss, J. High Energy Phys. 05 (2013) 086.
[53] D. Comelli, M. Crisostomi, and L. Pilo, J. High Energy Phys. 06 (2012) 085.
[54] F. Koennig, Y. Akrami, L. Amendola, M. Motta, and A. R. Solomon, Phys. Rev. D **90**, 124014 (2014).
[55] M. Lagos and P. G. Ferreira, J. Cosmol. Astropart. Phys. 12 (2014) 026.
[56] J. Stoer and R. Bulirsch, *Introduction to Numerical Analysis* (Springer-Verlag, Berlin, 1980).
[57] I. Gelfand, S. Fomin, and R. Silverman, *Calculus of Variations*, Dover Books on Mathematics (Dover Publications, New York, 2000).
[58] P. Pani, Int. J. Mod. Phys. A **28**, 1340018 (2013).
[59] E. Berti, V. Cardoso, and A. O. Starinets, Classical Quantum Gravity **26**, 163001 (2009).
[60] L. Lehner and F. Pretorius, arXiv:1106.5184.
[61] M. Kocic, M. Högås, F. Torsello, and E. Mortsell, arXiv:1708.07833.
[62] M. Högås, M. Kocic, F. Torsello, and E. Mörtsell, Classical Quantum Gravity **37**, 145010 (2020).
[63] S. W. Hawking and G. F. R. Ellis, *The Large Scale Structure of Space-Time*, Cambridge Monographs on Mathematical Physics (Cambridge University Press, Cambridge, England, 2011).
[64] C. Mazuet and M. S. Volkov, J. Cosmol. Astropart. Phys. 07 (2018) 012.
[65] B. Abbott *et al.* (LIGO Scientific, Virgo Collaborations), Phys. Rev. Lett. **116**, 061102 (2016).
[66] R. Abbott *et al.* (LIGO Scientific, Virgo Colllaborations), arXiv:2010.14527.
[67] R. Dong and D. Stojkovic, arXiv:2011.04032.